



Organosulfate produced from consumption of SO₃ speeds up sulfuric acid–dimethylamine atmospheric nucleation

Xiaomeng Zhang, Yongjian Lian, Shendong Tan, and Shi Yin

MOE Key Laboratory of Laser Life Science & Guangdong Provincial Key Laboratory of Laser Life Science & Guangzhou Key Laboratory of Spectral Analysis and Functional Probes, College of Biophotonics, South China Normal University, Guangzhou 510631, China

Correspondence: Shi Yin (yinshi@m.scnu.edu.cn)

Received: 18 July 2023 – Discussion started: 9 August 2023

Revised: 5 January 2024 – Accepted: 4 February 2024 – Published: 22 March 2024

Abstract. Although sulfuric acid (SA) and dimethylamine (DMA)-driven nucleation mainly dominates the new particle formation (NPF) process in the atmosphere, seeking the involvement of other gaseous species remains crucial for a better understanding of the NPF. Organosulfate has been detected in the gas phase and abundantly in atmospheric fine particles. However, its molecular formation mechanism and its impact on the NPF are still much less understood. Here, we explored the gas-phase reaction of glycolic acid (GA) with SO₃ and evaluated the enhancing potential of its products on the SA–DMA-driven NPF using a combination of quantum chemical calculations and kinetics modeling. We found that the considerable concentration of glycolic acid sulfate (GAS) is thermodynamically accessible from the reaction of GA with SO₃, efficiently catalyzed by SA or H₂O molecules. The produced GAS can form stable clusters with SA and DMA and speeds up the nucleation rate of the SA–DMA system obviously. Notably, the enhancement by GAS in the SA–DMA-based particle formation rate can be up to ~800 times in the region where the concentration of SA is about 10⁴ molec. cm⁻³. Supported by observations of atmospheric NPF events at Mt. Tai in China, our proposed ternary GAS–SA–DMA nucleation mechanism further indicates that the organosulfates produced from the consumption of SO₃ may play an important role in the unexpected high NPF rates observed in areas with relatively low concentrations of SA. The presented reaction and nucleation mechanisms provide a new feasible source of organosulfates in atmospheric new particles. Based on our findings, the impact of organosulfates on the atmospheric NPF in multiple regions around the world was estimated and discussed.

1 Introduction

Atmospheric aerosols have a significant influence on global climate, local air quality and human health (Wang et al., 2015, 2020; Lee et al., 2019; Zhang et al., 2004; Rose et al., 2018). New particle formation (NPF) in the atmosphere, including formation of a critical nucleus and subsequent growth of the nuclei, accounts for a significant fraction of secondary organic aerosols (SOA) (Rose et al., 2018; Yao et al., 2018; Zhang, 2010; Feketeová et al., 2019; Kirkby et al., 2016). It has been widely accepted that sulfuric acid (SA) is one of the most important nucleation precursors in the at-

mosphere (Zhang et al., 2004; Almeida et al., 2013; Kirkby et al., 2011; Loukonen et al., 2010; Zhao et al., 2011; Sipilä et al., 2010; X. Zhang et al., 2022; Olenius et al., 2017; Lehtipalo et al., 2016). Dimethylamine (DMA) was found to be one of the strongest species to enhance SA-driven NPF (Olenius et al., 2017; Yao et al., 2018). However, the binary SA–DMA-driven NPF still could not fully explain the observed NPF events globally, since there is still a gap between the observed particle formation rates and simulated rates (Kirkby et al., 2016; Shen et al., 2019; L. Liu et al., 2021; Shen et al., 2020). Therefore, seeking the involvement of other gaseous species to better understand the NPF has been paid

extensive attention in recent years (Olenius et al., 2017; Shen et al., 2019; Tan et al., 2022a; Ehn et al., 2014; Kawamura and Bikkina, 2016; Zhang et al., 2004).

Organic species commonly detected in aerosols are thought to play significant roles in particle formation and direct and indirect aerosol forcing (Jimenez et al., 2009; O'Dowd et al., 2002). Organosulfates have been identified as the most abundant class of organosulfur compounds, accounting for 5%–30% of the organic mass fraction in atmospheric particles (Brüggemann et al., 2017; Tolocka and Turpin, 2012; Shakya and Peltier, 2015; Froyd et al., 2010; Mutzel et al., 2015; Glasius et al., 2018). Katz et al. (2023) measured the presence of organosulfates and identified their importance for new particle formation. Ehn et al. (2010) made the first observation of gas-phase glycolic acid sulfate (GAS) in the Finnish forest, and GAS has been characterized and identified as the most abundant organosulfate in the fine particles collected from the southeastern USA (Hettiyadura et al., 2017). Various organosulfates have also been identified and characterized from fine particulate matter samples collected in the United States (Hettiyadura et al., 2015), China (Wang et al., 2018), Mexico City and Pakistan (Olson et al., 2011). These observed organosulfates represented by GAS and lactic acid sulfate are suggested to originate from the reaction of a variety of volatile organic compounds (Froyd et al., 2010; Darer et al., 2011; Riva et al., 2015; Kundu et al., 2013; H. Zhang et al., 2012; Zhang et al., 2014). However, despite extensive research and significant progress (Riva et al., 2015, 2016; Passananti et al., 2016; Ye et al., 2018; Zhu et al., 2019; McNeill, 2015, 2012), huge areas of uncertainty remain in the current understanding of organosulfates, their molecular formation pathways and their impacts on the atmospheric NPF (Brüggemann et al., 2020).

Organic acids, which are frequently observed in the atmosphere, have been expected to participate in the process of atmospheric nucleation, with a focus on the thermochemical properties of clusters between organic acids and common atmospheric nucleation precursors (R. Zhang et al., 2022). Glycolic acid (GA) as the simplest α -hydroxy acid is a highly oxidized multifunctional organic acid and has been detected in diverse environments with a relatively high concentration (Miyazaki et al., 2014; Mochizuki et al., 2019; Brüggemann et al., 2017). For example, Mochizuki et al. (2017) found that the maxima of GA in the gas phase could be up to 343 ng m^{-3} at Mt. Tai in North China and showed that the gas-phase concentrations of the total monoacids including GA and lactic acid are higher than those of the particle phase. Miyazaki et al. (2014) detected the presence of GA in the gas phase within the marine atmospheric boundary layer over the western subarctic North Pacific. Interestingly, organic compounds with the -OH or -COOH group have been proven to have a highly reactive activity with SO_3 (Li et al., 2018; Mitsui et al., 2011; Zhuang and Pavlish, 2012), which is a major air pollutant and is mainly emitted from the gas-phase oxidation of SO_2 (Mitsui et al., 2011; Chen and Bhattacharya, 2013;

Cao et al., 2010; Zhong et al., 2018). Due to the presence of polar functional groups (-OH and -COOH groups), the two active sites of α -hydroxy acid can react with SO_3 to form carboxylic acid sulfates and carboxylic acid sulfuric anhydrides, individually (Tan et al., 2022b; Liu et al., 2019; Mackenzie et al., 2015; Smith et al., 2017, 2018, 2019; Shen et al., 1990). A recent computational study probed the cluster formation mechanism of GA-SA and NH_3 and showed that GA acts as a mediate bridge for the formation of SA- NH_3 -based clusters (Zhang et al., 2017). Organic sulfur species, mainly including organosulfates (Nguyen et al., 2014) and carboxylic sulfuric anhydrides (H. J. Zhang et al., 2018; Rong et al., 2020; H. Zhang et al., 2022) with a relatively lower vapor pressure, have also been inferred as facilitating the occurrence of NPF in the atmosphere. However, although many studies have illustrated that atmospheric organic species produced by a gas-phase chemical reaction can exert a significant influence on atmospheric NPF processes (R. Zhang et al., 2012; L. Liu et al., 2018; Wang et al., 2010; Hirvonen et al., 2018; Laaksonen et al., 2008; Ristovski et al., 2010; Metzger et al., 2010), the cluster formation mechanism of GAS, produced from the reaction of GA and SO_3 with the typical nucleation precursors SA and DMA, has never been systematically investigated and compared.

In current research, we performed a comparative study on GA as well as its products (GAS and glycolic acid sulfuric anhydride – GASA) to probe the role of organic acid, organosulfate and organic sulfuric anhydride in enhancing the SA-DMA nucleation potential by evaluating the formation mechanism of the GA-SA-DMA, GAS-SA-DMA and GASA-SA-DMA systems. We have obtained the minimum free energy structures of the $(\text{GA})_x(\text{SA})_y(\text{DMA})_z$, $(\text{GAS})_x(\text{SA})_y(\text{DMA})_z$ and $(\text{GASA})_x(\text{SA})_y(\text{DMA})_z$ ($0 \leq z \leq x + y \leq 3$) systems. The kinetics of the cluster formation pathways and rates were obtained via the ACDC simulations, which use the calculated thermodynamic data of acquired clusters as input (McGrath et al., 2012; Olenius et al., 2013). The simulated particle formation rates of the GAS-involved system were compared with those of the GA- and GASA-involved systems based on the corresponding observational concentration (Stieger et al., 2021; Miyazaki et al., 2014; Mochizuki et al., 2017, 2019). Additionally, we also compared the calculated ternary GAS-SA-DMA nucleation rates with the field observations of NPF at Mt. Tai in China and found that the ternary nucleation mechanism-involved GAS was well supported by the observations. Finally, the impact of the organosulfates on the atmospheric NPF in multiple regions around the world was estimated and discussed.

2 Method

2.1 Configurational sampling

A multistep global minimum sampling scheme, which has previously been applied to study the atmospheric

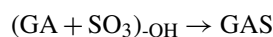
cluster formation (Ma et al., 2019), was employed to search for the global minima of the $(\text{GA})_x(\text{SA})_y(\text{DMA})_z$, $(\text{GAS})_x(\text{SA})_y(\text{DMA})_z$ and $(\text{GASA})_x(\text{SA})_y(\text{DMA})_z$ ($0 \leq z \leq x + y \leq 3$) clusters. The global minimum structures of the GA, GAS and GASA molecules were taken from a previous study (Tan et al., 2022b). To locate the global minimum energy structure, the artificial bee colony algorithm was systematically employed by the ABCCluster program to generate 1000 initial random configurations for each cluster (Zhang and Dolg, 2015), and then these configurations were further pre-optimized using the PM7 semi-empirical method implemented in the MOPAC2016 program (Stewart, 2007, 2013, 2016). Second, up to 100 structures with relatively lower energies were selected from the 1000 structures, and a M06-2X/6-31+G* level of theory was applied for subsequent optimization. Finally, further geometry optimization and frequency calculations at the M06-2X/6-311++G(3df,3pd) level of theory were performed to optimize the 10 best of 100 optimized configurations, and then the global minimum structure with the lowest energy was obtained.

2.2 Quantum chemical calculations

All the density functional theory (DFT) calculations were implemented in the GAUSSIAN 09 program package (Frisch et al., 2009). The M06-2X function combined with the 6-311++G(3df,3pd) basis set was chosen as it has been proven to be accurate in estimating the thermodynamic properties of atmospheric clusters, such as organic acid–SA–amine clusters, amide–SA clusters or amino acid–SA clusters (Clark et al., 1983; Elm et al., 2012; Herb et al., 2011; Elm et al., 2015, 2016; Ge et al., 2018a, b). Intrinsic reaction coordinate (IRC) calculations were carried out to verify the connections of the transition states with the reactants and products. Single-point energies were calculated at the DLPNO-CCSD(T)/aug-cc-pVTZ level based on the optimized geometries using the ORCA 4.1.2 package (Riplinger and Neese, 2013; Riplinger et al., 2013; Neese, 2012; Lu, 2022), which has gained popularity in large cluster formation studies (Xie et al., 2017; Chen et al., 2020; Shen et al., 2019). Zero-point energies at the M06-2X/6-311++G(3df,3pd) level were performed to correct for the corresponding single-point energies. The corresponding formation Gibbs free energies of the stable clusters are summarized in the Supplement.

2.3 The concentration of GAS and GASA

The formation of GAS and GASA can be described by the following two reactions.



The equilibrium constant $K_{(\text{GA}+\text{SO}_3)_{\text{OH}}}$ for the formation of GAS and $K_{(\text{GA}+\text{SO}_3)_{\text{COOH}}}$ for the formation of GASA are

$$K_{(\text{GA}+\text{SO}_3)_{\text{OH}}} = \frac{[\text{GAS}]}{[\text{GA}][\text{SO}_3]} = e^{\frac{-\Delta G}{RT}},$$

$$K_{(\text{GA}+\text{SO}_3)_{\text{COOH}}} = \frac{[\text{GASA}]}{[\text{GA}][\text{SO}_3]} = e^{\frac{-\Delta G}{RT}},$$

and the equilibrium concentration of GAS and GASA can be roughly estimated theoretically using the following expressions:

$$[\text{GAS}] = K_{(\text{GA}+\text{SO}_3)_{\text{OH}}}[\text{GA}][\text{SO}_3],$$

$$[\text{GASA}] = K_{(\text{GA}+\text{SO}_3)_{\text{COOH}}}[\text{GA}][\text{SO}_3],$$

where $K_{(\text{GA}+\text{SO}_3)_{\text{OH}}}$ and $K_{(\text{GA}+\text{SO}_3)_{\text{COOH}}}$ are equal to the equilibrium constants from the formation Gibbs energies of the GAS and GASA, respectively. $[\text{GA}]$ and $[\text{SO}_3]$ are the concentrations of the GA and SO_3 monomer, respectively. We use the reactant concentrations of $[\text{GA}] = 1.11 \times 10^7 - 2.72 \times 10^9 \text{ molec. cm}^{-3}$ according to the values of some field observations (Mochizuki et al., 2019; Miyazaki et al., 2014; Stieger et al., 2021; Mochizuki et al., 2017). Considering atmospheric SO_3 field measurements (Yao et al., 2020), its concentration is considered in the range of $10^4 - 10^6 \text{ molec. cm}^{-3}$. Based on the above equations, the estimated concentration of the reaction product, GAS, is about $2.14 \times 10^2 - 5.24 \times 10^6 \text{ molec. cm}^{-3}$, and the GASA is about $2.30 \times 10^{-7} - 5.62 \times 10^{-3} \text{ molec. cm}^{-3}$. Thus, a range of concentrations for the GAS, from 10^2 to $10^6 \text{ molec. cm}^{-3}$, is selected for the discussion in this work (Fig. 3, Table S1 and Fig. S9 in the Supplement).

2.4 Atmospheric cluster dynamics code (ACDC) kinetic model

The ACDC simulations form a dynamical model where the time development of molecular cluster concentrations is solved by integrating numerically the birth–death equations using the MATLAB-R2019b program (McGrath et al., 2012; Olenius et al., 2013; Ortega et al., 2012; Shampine and Reichelt, 1997). In the current research, the ACDC was employed to investigate the formation pathways and formation rates of the clusters. The birth–death equations can be written as

$$\frac{dc_i}{dt} = \frac{1}{2} \sum_{j < i} \beta_{j,(i-j)} c_j c_{(i-j)} + \sum_j \gamma_{(i+j) \rightarrow i} c_{i+j} - \sum_j \beta_{i,j} c_i c_j - \frac{1}{2} \sum_{j < i} \gamma_{i \rightarrow j} c_i + Q_i - S_i, \quad (1)$$

where i and j are the clusters given in the system, c_i and c_j are the concentrations of clusters i and j , $\beta_{i,j}$ is the collision coefficient between clusters i and j , and $\gamma_{(i+j) \rightarrow i}$ is the evaporation coefficient of cluster $(i + j)$ evaporating into

clusters i and j . Q_i is the possible additional sources of cluster i , and S_i is the sink term for taking into account external losses of cluster i . The collision coefficient β is calculated using the kinetic gas theory as Eq. (2) (taking $\beta_{i,j}$ as an example):

$$\beta_{ij} = \left(\frac{3}{4\pi}\right)^{1/6} \left(\frac{6k_bT}{m_i} + \frac{6k_bT}{m_j}\right)^{1/2} \left(V_i^{1/3} + V_j^{1/3}\right)^2, \quad (2)$$

where k_b is the Boltzmann constant; T is the temperature; m_i and m_j are the masses of i and j , respectively; and V_i and V_j are their respective volumes. The evaporation coefficient $\gamma_{(i+j) \rightarrow i}$ is calculated using the Gibbs free energies of the formation of the clusters

$$\gamma_{(i+j) \rightarrow i} = \beta_{ij} \frac{c_i^e c_j^e}{c_{i+j}^e} = \beta_{ij} c_{\text{ref}} \exp\left\{-\frac{\Delta G_{i+j} - \Delta G_i - \Delta G_j}{k_b T}\right\}, \quad (3)$$

where c_i^e is the equilibrium concentration of cluster i , ΔG_i is the Gibbs free energy of the formation of cluster i , and c_{ref} is the monomer concentration at the reference vapor corresponding to the pressure of 1 atm at which the Gibbs free energies were determined.

Here, the ACDC simulation system is regarded as a “3 × 3” box containing the $(\text{GA})_x(\text{SA})_y(\text{DMA})_z$, $(\text{GAS})_x(\text{SA})_y(\text{DMA})_z$ and $(\text{GASA})_x(\text{SA})_y(\text{DMA})_z$ (where the total number of x and y is from 0 to 3 and z from 0 to 3) clusters. Among these clusters, only the clusters including an equal number of z and $x + y$ or the clusters with smaller numbers of z and $x + y$ were considered, as only these clusters have the potential to further grow into larger sizes (Li et al., 2018; Olenius et al., 2013).

A detailed description of the boundary clusters that are allowed to leave the simulation and contribute to NPF is presented in the Supplement. In the current study, $[\text{GA}]$ ranged from 10^7 to 10^{10} molec. cm^{-3} , and the corresponding $[\text{GAS}]$ was 10^3 – 10^6 molec. cm^{-3} (Miyazaki et al., 2014; Mochizuki et al., 2017, 2019; Stieger et al., 2021). A constant coagulation sink of $2.6 \times 10^{-3} \text{ s}^{-1}$ was applied to account for scavenging by larger particles. The simulations were mainly run at 278 K, with additional runs at 258 and 298 K to investigate the influence of temperature. These conditions correspond to a typical sink value and temperature in the boreal forest environment (Olenius et al., 2013; Dal Maso et al., 2008).

3 Results and discussion

3.1 The reaction of GA with SO_3

The potential energy surfaces (PESs) of the reaction between GA and SO_3 , along with the optimized structures of the pre-reaction complexes (R), transition states (TSs) and products (P), are presented in Fig. 1. Since GA contains both the -OH and -COOH functional groups, two reaction pathways for GA and SO_3 are considered in this study: (1) the esterification reaction between the hydroxyl group of GA and SO_3

[[$(\text{GA} + \text{SO}_3)_{\text{-OH}}$] and (2) the cycloaddition reaction between the carboxyl group of GA and SO_3 [[$(\text{GA} + \text{SO}_3)_{\text{-COOH}}$]. In the presumed reaction pathway (1) (without a catalyst), the hydroxyl oxygen atom of GA could react with the sulfur atom of SO_3 to form sulfate GAS (Fig. 1a), followed by simultaneous proton transfer from GA to SO_3 . However, the Gibbs free energy barrier is $23.08 \text{ kcal mol}^{-1}$, which shows that a direct reaction between the hydroxyl group and SO_3 is a thermodynamically unfavorable pathway for the formation of GAS. The high-energy barrier of the $(\text{GA} + \text{SO}_3)_{\text{-OH}}$ reaction partly ascribes to the ring tension a rather closed four-membered ring transition state structure. Differently, the Gibbs free energy barrier of the $(\text{GA} + \text{SO}_3)_{\text{-COOH}}$ reaction path without a catalyst is significantly lower, only 3 kcal mol^{-1} (Fig. 1b).

With a high abundance ($\sim 10^{17} \text{ cm}^{-3}$) being detected in the troposphere (Huang et al., 2015), H_2O has been reported as effectively acting as a catalyst in chemical reactions (Liu et al., 2019). Herein, we investigated the catalytic effect of H_2O on the reaction of GA and SO_3 . As can be seen in Fig. 1a, the free energy barrier of the $(\text{GA} + \text{SO}_3)_{\text{-OH}}$ reaction catalyzed by H_2O is $3.41 \text{ kcal mol}^{-1}$, which is substantially lower than that for the direct reaction without a catalyst. The free energy barrier for the H_2O -catalyzed $(\text{GA} + \text{SO}_3)_{\text{-COOH}}$ reaction is $0.92 \text{ kcal mol}^{-1}$. These results indicate that both reaction pathways for GA + SO_3 are favorable with the catalysis of H_2O to generate GAS and GASA, respectively. Therefore, as the relative humidity (RH) increases, it should be conducive to the formation of GAS and GASA. The abundances of hydrated GA clusters $\text{GA}-n(\text{H}_2\text{O})$ ($n = 0$ –3) were also calculated at different RHs (Fig. S3 and Table S3). The relative equilibrium abundance of GA hydrates is less than 7% at RH = 90% and 298 K. Since the hydration of GA is weak, the effect of the hydrated GA clusters on the formation of GAS and GASA is not considered further. SA can also act as both an acceptor and a donor of hydrogen, thereby promoting various proton transfer reactions to facilitate the formation of GAS and GASA with a low barrier (Yao et al., 2018; Liu et al., 2017; Tan et al., 2018). As shown in Fig. 1a (black line), the energy barrier of the GA + SO_3 reaction in the presence of the catalyst SA sharply decreases with the value of $2.83 \text{ kcal mol}^{-1}$ for the formation of GAS and with that of $1.13 \text{ kcal mol}^{-1}$ for the formation of GASA (black line in Fig. 1b). As the geometry structures of the transition states (TS1 to TS6) shown in Fig. 1, the participation of the catalysts could efficiently decrease the ring tension of the transition state geometry by increasing the ring size, followed by the reduction in the related energy barrier.

Hence, the catalysts H_2O or SA could make the GA + SO_3 reaction barrier-less and readily occur in the atmosphere. Indeed, many SO_3 -involved gas-phase reactions can be effectively catalyzed by H_2O or SA (Li et al., 2018; Liu et al., 2019). Note that previous computational studies have proved that organic acids can act as catalysts for the reaction of SO_3 and H_2O to form sulfuric acid (Hazra and Sinha,

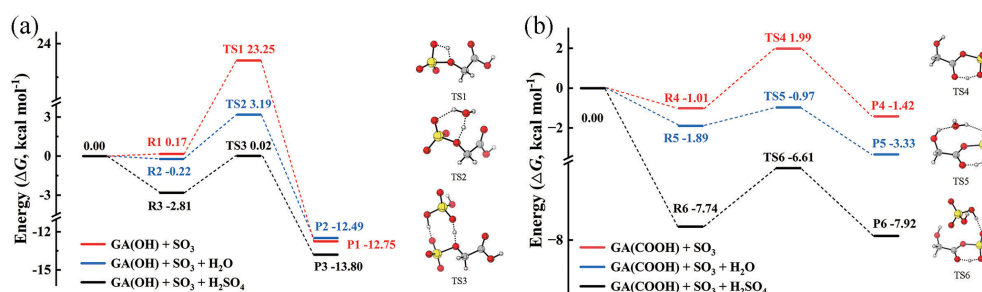


Figure 1. Potential energy surfaces at the DLPNO-CCSD(T)/aug-cc-pVTZ//M06-2X/6-311++G(3df,3pd) level of theory (kcal mol^{-1}) (at 298 K, 1 atm) for the gas-phase reactions of GA and SO_3 through paths (a) SO_3 attacking the $-\text{OH}$ group of GA and (b) SO_3 attacking the $-\text{COOH}$ group of GA. The red line represents the reaction without a catalyst, the blue line represents the reaction with H_2O as a catalyst, and the black line represents the reaction with H_2SO_4 as a catalyst. R, TS and P refer to the pre-reaction complex, transition state and product, respectively. The hydrogen, carbon, oxygen and sulfur atoms are represented by the white, gray, red and yellow spheres, respectively.

2011). Although we pay more attention to the catalytic effect of H_2O on the reaction of α -hydroxy acid with SO_3 in this study, the possible pathway of GA catalyzing the $\text{SO}_3 + \text{H}_2\text{O} \rightarrow \text{SA}$ reaction should not be ignored. Its PES (black line) is considered and compared with H_2O catalytic reaction paths (see the details in Fig. S1 and the related discussions in the Supplement). It is worth noting that the product GAS generated from GA and SO_3 , with a more negative Gibbs free energy of formation ($-12.75 \text{ kcal mol}^{-1}$), is more stable than the product GASA ($-1.42 \text{ kcal mol}^{-1}$) as displayed in Fig. 1. This may suggest a possible formation pathway for the gas-phase GAS observed in the atmosphere. To the best of our knowledge, the gas-phase GAS has been detected for the first time in the Finnish boreal forest (Ehn et al., 2010). Le Breton et al. (2018) identified and measured 17 sulfur-containing organics (including organosulfates, and GAS is one of them) at a regional site 40 km northwest of Beijing. They successfully identified a persistent gas-phase presence of organosulfates in the ambient air. The mean contribution from gas-phase sulfur-containing organics to the total was found up to be 11.6% and $\sim 23 \text{ ng m}^{-3}$. Ye et al. (2021) also detected the ion $\text{C}_2\text{H}_3\text{SO}_6^-$ with a diurnal peak in the afternoon in both the gas phase and the particle phase, whose ion was attributed to GAS, in Guangzhou in southern China during the fall of 2018. Unfortunately, atmospheric field observation data on gas-phase organosulfates and organic sulfuric anhydrides are still relatively scarce. In order to explore their impacts on the atmospheric NPF, we calculated the atmospheric concentrations of the GAS and GASA based on the thermodynamic equilibrium of the chemical reactions. The estimated concentration of GAS is in the range of 10^3 – $10^5 \text{ molec. cm}^{-3}$, and that of GASA is $\sim 10^{-6}$ – $10^{-4} \text{ molec. cm}^{-3}$ (see the details in Table S1 and the first part of the Supplement).

3.2 Cluster thermodynamic data

In order to evaluate the enhancing potential of GA and its different reaction products GAS and GASA in the typical SA–DMA-driven NPF process, we analyzed the global

minima of the GA–SA–DMA, GAS–SA–DMA and GASA–SA–DMA clusters. The identified lowest free energy structures of the $(\text{GA})_x(\text{SA})_y(\text{DMA})_z$, $(\text{GAS})_x(\text{SA})_y(\text{DMA})_z$ and $(\text{GASA})_x(\text{SA})_y(\text{DMA})_z$ ($0 \leq z \leq x + y \leq 3$) clusters are depicted in Figs. S4, S5 and S6, respectively. In general, both intermolecular hydrogen bond and ion electrostatic interactions formed by proton transfer reactions are found to play a key role in stabilizing these clusters. Hydrogen bond interactions are observed in all the clusters. The $-\text{OH}/-\text{COOH}$ group in GA/GAS/GASA participates in at least one hydrogen bond formation and acts as a donor or acceptor of hydrogen. The proton transfer reactions that generally occurred in the acid–base clusters are found in most of the DMA-containing heteromolecular clusters but are not observed in the acidic homomolecular $(\text{GA})_x$, $(\text{GAS})_x$ and $(\text{GASA})_x$ ($x = 1$ – 3) clusters and the GA–SA, GAS–SA and GASA–SA clusters, in which only hydrogen bond interactions are found. Interestingly, there is no proton transfer in the $(\text{GA})_1(\text{DMA})_1$, $(\text{GAS})_1(\text{DMA})_1$ and $(\text{GASA})_1(\text{DMA})_1$ clusters. However, when another extra molecule is added to these three clusters, not only is the hydrogen bond interaction enhanced, but the proton is also transfer-promoted. This is because the trimer or large clusters are sufficient for converting a hydrogen-bonded system to an ion electrostatic interaction system, a consequence of proton transfer reaction.

The formation Gibbs free energies ΔG and evaporation rate values of the GA–SA–DMA, GAS–SA–DMA and GASA–SA–DMA clusters are obtained along with the acquisition of global minimum structures. More details about the ΔG and evaporation rates are shown in Tables S4–S6 and Fig. S7. Previous studies have verified that DMA is one of the strongest compounds for stabilizing SA clusters (Yao et al., 2018; Almeida et al., 2013; Jen et al., 2014). Since the $(\text{SA})_3(\text{DMA})_3$ cluster is the most stable cluster of the SA–DMA system, its ΔG and evaporation rate were taken as a reference value for comparison. In Fig. 2, the formation free energies ΔG (orange histograms) and evaporation rates $\sum \gamma$ (black points) at 278 K of the $(\text{SA})_3(\text{DMA})_3$

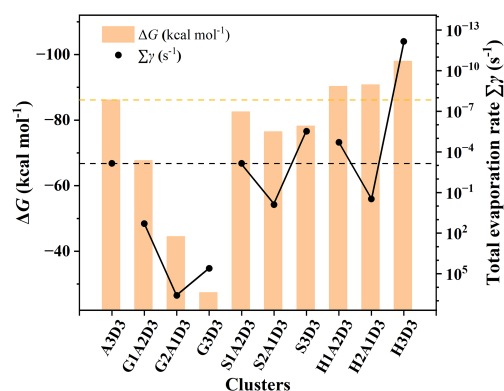


Figure 2. The formation Gibbs free energies ΔG (kcal mol^{-1}) and evaporation rates $\sum \gamma$ (s^{-1}) of the $(\text{GA})_x(\text{SA})_y(\text{DMA})_3$, $(\text{GAS})_x(\text{SA})_y(\text{DMA})_3$ and $(\text{GASA})_x(\text{SA})_y(\text{DMA})_3$ ($x = 0-3$, $x + y = 3$) clusters calculated at the DLPNO-CCSD(T)/aug-cc-pVTZ//M06-2X/6-311++G(3df,3pd) level of theory and 278 K. DMA, SA, GA, GAS and GASA are represented by D, A, G, S and H, individually.

cluster are presented along with the $(\text{GA})_x(\text{SA})_y(\text{DMA})_3$, $(\text{GAS})_x(\text{SA})_y(\text{DMA})_3$ and $(\text{GASA})_x(\text{SA})_y(\text{DMA})_3$ ($x = 0-3$, $x + y = 3$) clusters as a comparison. The ΔG of the $(\text{GA})_{1-3}(\text{SA})_{0-2}(\text{DMA})_3$ clusters are in all cases much more positive than that of the $(\text{SA})_3(\text{DMA})_3$ cluster, within a difference in the range of 18.49–58.74 kcal mol^{-1} . For the $(\text{GAS})_{1-3}(\text{SA})_{0-2}(\text{DMA})_3$ clusters, their ΔG is close to that of the $(\text{SA})_3(\text{DMA})_3$ cluster, which is slightly negative, and the difference is in the range of 3.61–9.69 kcal mol^{-1} . Notably, the ΔG of the $(\text{GASA})_{1-3}(\text{SA})_{0-2}(\text{DMA})_3$ clusters becomes more negative than that of the $(\text{SA})_3(\text{DMA})_3$ cluster. Their value discrepancies are -4.13 , -4.63 and -11.83 kcal mol^{-1} , respectively, with the number of the GASA increasing from 1 to 3. The above results indicate that the various organic compounds generated via the chemical reaction, such as GA and its products GAS and GASA, can apparently lead to different formation Gibbs free energies of clusters with the same scale when participating in the nucleation of the SA–DMA system due to their unequal intermolecular hydrogen bond and ion electrostatic interaction capacities with acidic and basic molecules, respectively.

The comparison of the evaporation rates of these clusters is more interesting. For the $(\text{Org})_x(\text{SA})_y(\text{DMA})_3$ ($\text{Org} = \text{GA, GAS and GASA}$; $x = 1-3$, $x + y = 3$) clusters, the evaporation rate of $(\text{Org})_x(\text{SA})_y(\text{DMA})_3$ does not simply change with the increasing number of organic molecules. The evaporation rate of $(\text{Org})_2(\text{SA})(\text{DMA})_3$ ($\text{Org} = \text{GA, GAS and GASA}$) is largest. The evaporation rates of the $(\text{GAS})_1(\text{SA})_2(\text{DMA})_3$, $(\text{GAS})_3(\text{DMA})_3$, $(\text{GASA})_1(\text{SA})_2(\text{DMA})_3$ and $(\text{GASA})_3(\text{DMA})_3$ clusters vary from 10^{-13} to 10^{-4} s^{-1} , which are smaller than that of the $(\text{SA})_3(\text{DMA})_3$ cluster, implying that the substitutions of one or three SAs by the GAS and GASA molecules are benefi-

cial for stabilizing clusters. However, the evaporation rates of the GA–SA–DMA clusters are found to be largest when comparing them with that of the corresponding GAS–SA–DMA, GASA–SA–DMA and $(\text{SA})_3(\text{DMA})_3$ clusters displayed in Fig. 2. Actually, the evaporation rates of all the GA–SA–DMA clusters we calculated are larger than 10^1 s^{-1} (Fig. S7), indicating the instability of the participation of GA in the SA–DMA cluster system. The more negative ΔG and smaller evaporation rates of the GAS/GASA–SA–DMA clusters suggest that they are thermodynamically more favorable than the GA–SA–DMA system in the cluster formation process, resulting from the greater binding ability between the GAS–GASA and SA–DMA systems than that between the GA and SA–DMA systems. Hence, we can draw an initial conclusion that the GAS or GASA produced from a GA + SO_3 reaction may efficiently stabilize the SA–DMA system, in contrast to GA itself.

3.3 Cluster formation rates

The corresponding formation rates of the clusters in the GA–SA–DMA, GAS–SA–DMA and GASA–SA–DMA systems were further investigated and compared to achieve a deeper understanding of the influence of GA/GAS/GASA on the SA–DMA-based system using ACDC simulations. Figure 3 presents the comparison of the cluster formation rate as a function of the concentration of GA (1.1×10^7 – 2.7×10^9 molec. cm^{-3}), GAS (2.1×10^3 – 5.2×10^5 molec. cm^{-3}) and GASA (2.3×10^{-6} – 5.6×10^{-4} molec. cm^{-3}) for the Org–SA–DMA systems at 278 and 258 K, under the condition of $[\text{SA}] = 10^5$ molec. cm^{-3} . The concentration of DMA is selected to be 10^8 molec. cm^{-3} , according to the typical concentrations observed in the gas phase in high mountains (F. Liu et al., 2018; Matsumoto et al., 2023). To compare the enhancing potential of GAS and GA on the SA–DMA-based NPF, Fig. 3a presents the cluster formation rates as a function of $[\text{GAS}]$ and $[\text{GA}]$ at 278 K. The cluster formation rate of the GAS–SA–DMA system markedly increases with the increasing concentration of $[\text{GAS}]$ compared to that of the GA–SA–DMA system, especially in the case of $[\text{GAS}] > 3 \times 10^4$ molec. cm^{-3} . As the concentration of GAS increased from 2.1×10^3 to 5.2×10^5 molec. cm^{-3} , the cluster formation rate of the GAS–SA–DMA system yields a 10-fold increase (Fig. 3a), whereas the cluster formation rate of the GA–SA–DMA system basically remains unchanged (from $\sim 3.48 \times 10^{-3}$ to $\sim 3.52 \times 10^{-3}$ $\text{cm}^{-3} \text{s}^{-1}$, as displayed more clearly in Fig. 3b) with the increase in the corresponding concentration of GA. Although the concentration of GAS is typically 4 orders of magnitude lower than that of GA, it has a significantly higher enhancing potential than GA in the SA–DMA-based nucleation system. The cluster formation rate as a function of $[\text{GASA}]$ for the GASA–SA–DMA system is also compared with that of $[\text{GA}]$ for the GA–SA–DMA system at 278 K in Fig. 3b. The growing trend of the cluster formation rate for the

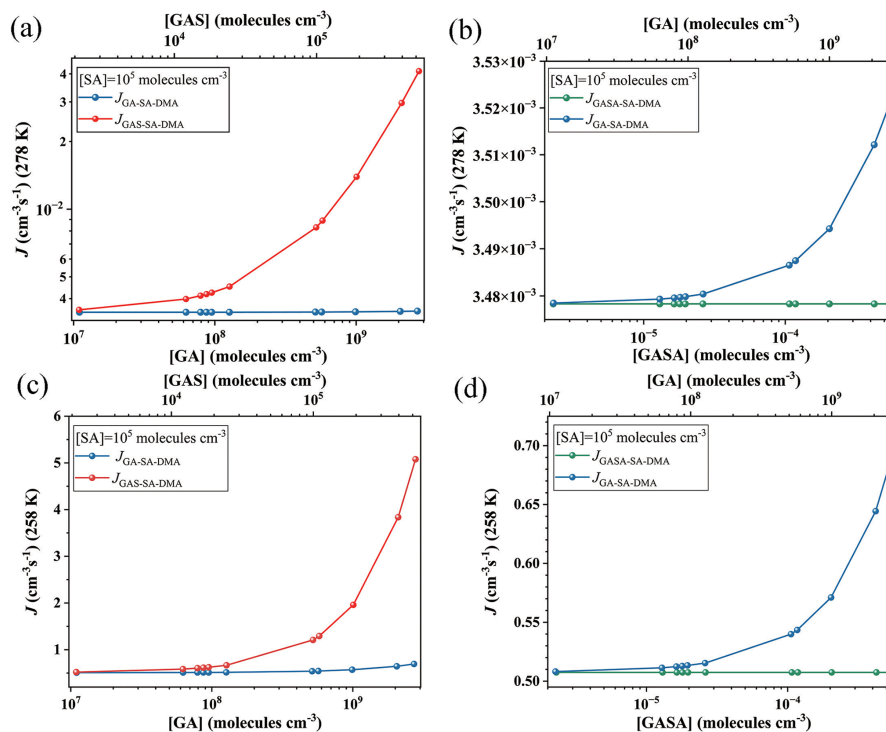


Figure 3. Simulated cluster formation rates J ($\text{cm}^{-3} \text{s}^{-1}$) as a function of monomer concentrations ($[\text{GA}]$, $[\text{GAS}]$ and $[\text{GASA}]$, respectively) at **(a, b)** 278 K and **(c, d)** 258 K under the condition of $[\text{DMA}] = 10^8 \text{ molec. cm}^{-3}$ and $[\text{SA}] = 10^5 \text{ molec. cm}^{-3}$. Note that the simulated $J_{\text{GA-SA-DMA}}$ are the same data, but the y-axis scales are different at panels **(a)**, **(b)**, **(c)** and **(d)**, individually.

GASA–SA–DMA system is even smaller than that for the GA–SA–DMA system. Combined with the cluster thermodynamic results discussed in the previous section, we can conclude that such different trends should be responsible for the combined impact of the cluster ΔG , cluster evaporation rate and organic species concentration of these systems, respectively. The most rapid increasing trend of the cluster formation rate of the GAS–SA–DMA system is a consequence of the favorable ΔG and low evaporation rates of the $(\text{GAS})_x(\text{SA})_y(\text{DMA})_z$ clusters and the non-low-equilibrium concentration of GAS. The unfavorable ΔG and large evaporation rates of the $(\text{GA})_x(\text{SA})_y(\text{DMA})_z$ clusters make the GA–SA–DMA system kinetically unfavorable, even with a high GA concentration. For the trend of the GASA–SA–DMA system, the extremely low-equilibrium concentration of GASA makes its cluster formation rate hard to promote, even with the thermodynamically favorable conditions for the $(\text{GASA})_x(\text{SA})_y(\text{DMA})_z$ cluster formation. $[\text{SO}_3] = 10^4$ and $10^6 \text{ molec. cm}^{-3}$ are also considered and compared with the results shown in Fig. 3a (as displayed in Fig. S9). In the case of $[\text{SO}_3] = 10^4 \text{ molec. cm}^{-3}$, it is worth noting that the cluster formation rate of the GAS–SA–DMA system slightly increases with the increasing $[\text{GAS}]$ compared to that of the GA–SA–DMA system with a corresponding $[\text{GA}]$, where $J_{\text{GAS-SA-DMA}}$ reaches twice the value of $J_{\text{GA-SA-DMA}}$. For $[\text{SO}_3] = 10^6 \text{ molec. cm}^{-3}$, the trend of this difference be-

comes relatively obvious, and $J_{\text{GAS-SA-DMA}}$ grows up to 2 orders of magnitude higher than $J_{\text{GA-SA-DMA}}$.

The effects of temperature and SA concentration on the cluster formation rates of these systems were also explored. As the temperature decreases to 258 K (Fig. 3c and d), the cluster formation rates of all the considered systems increase by about 2 to 3 orders of magnitude compared to that of 278 K. This behavior mainly results from the clusters becoming thermodynamically favorable at relatively low temperatures, making the clusters more stabilized. The simulated cluster formation rates J ($\text{cm}^{-3} \text{s}^{-1}$) of these systems under different $[\text{SA}]$ (10^4 , 10^6 and $10^7 \text{ molec. cm}^{-3}$) at 278 K are presented in Fig. S8. Their increasing trends of cluster formation rates as a function of organic species concentration are consistent with those obtained above at $[\text{SA}] = 10^5 \text{ molec. cm}^{-3}$. The cluster formation rates of these systems also become large with an $[\text{SA}]$ increase. For example, the highest cluster formation rate of the GAS–SA–DMA system is $\sim 4 \times 10^{-2} \text{ cm}^{-3} \text{s}^{-1}$ within the considered GAS concentration at 278 K when $[\text{SA}] = 10^5 \text{ molec. cm}^{-3}$ (Fig. 3a), while this value could be up to $2.1 \times 10^3 \text{ cm}^{-3} \text{s}^{-1}$ when $[\text{SA}]$ increases to $10^7 \text{ molec. cm}^{-3}$ (Fig. S8). These results suggest that the particle formation rate of the GAS-involved SA–DMA system tends to become even larger under low-temperature and high-sulfuric-acid-concentration conditions.

3.4 Enhancement effect of GAS on NPF

To further evaluate the enhancement potential of GAS on the SA–DMA-driven NPF, $J_{\text{GAS-SA-DMA}}$ and $J_{\text{SA-DMA}}$ are compared by defining a ratio r_{GAS} , which stands for the ratio of the cluster formation rate with GAS to that without GAS:

$$r_{\text{GAS}} = \frac{J([\text{GAS}] = x, [\text{SA}] = y, [\text{DMA}] = z)}{J([\text{SA}] = y, [\text{DMA}] = z)}, \quad (4)$$

where [GAS], [SA] and [DMA] represent monomer concentrations of GAS, SA and DMA, respectively. r_{GAS} was calculated under the conditions of $[\text{GAS}] = 10^3$ to $\sim 10^5$ molec. cm^{-3} , $[\text{SA}] = 10^4$ – 10^7 molec. cm^{-3} and $[\text{DMA}] = 10^8$ molec. cm^{-3} , which are the typical observed values in the atmosphere (Li et al., 2018; Riipinen et al., 2007; Kürten et al., 2014; Ge et al., 2011).

Figure 4 shows the enhancement strength r_{GAS} , which presents a dependence on [GAS] and [SA]. The r_{GAS} increases with the increase in [GAS] and can reach as high as ~ 800 at 278 K with $[\text{GAS}] \simeq 10^5$ molec. cm^{-3} and $[\text{SA}] \simeq 10^4$ molec. cm^{-3} , suggesting that the GAS can substantially enhance the formation rates of the SA–DMA-driven NPF, especially under relevant low [SA] atmospheric conditions. For instance, low concentrations of SA $\sim 10^4$ molec. cm^{-3} together with relatively high NPF rates (5 – 9 $\text{cm}^{-3} \text{s}^{-1}$) were observed at Hyytiälä in Finland and Hohenpeissenberg in Germany (Mikkonen et al., 2011; Birmili et al., 2003; Dal Maso et al., 2007). Since relatively high concentrations of hydroxy acids (259 ng m^{-3}) were also observed in the same period in nearby regions (Stieger et al., 2021), the new particles may be mainly formed through the ternary GAS–SA–DMA pathway rather than the SA–DMA pathway in these scenarios. With the [SA] increase, the r_{GAS} becomes smaller as shown in Fig. 4. This is likely due to the abundance advantage of SA compared to GAS in the concentration range we considered. When their concentrations are equal, GAS exhibits a certain enhancement effect. For example, r_{GAS} still can reach ~ 3 with the condition of $[\text{GAS}] = [\text{SA}] = 10^5$ molec. cm^{-3} , which indicates that the nucleation capability between GAS and DMA is not inferior to that of SA and DMA when the concentration of GAS and SA is at the same level. Previous studies have shown that the concentrations of organic precursors are usually several orders of magnitude higher than that of SA, when the enhancement strength r is slightly larger than 1 (Li et al., 2017; J. R. Liu et al., 2021; H. Zhang et al., 2018). For example, the enhancement effect of lactic acid (LA) on the SA–DMA-driven NPF at 260 K is approximately equal to 1 under the condition of $[\text{LA}] = 10^{10}$ and $[\text{SA}] = 10^5$ molec. cm^{-3} (Li et al., 2017). Overall, this suggests that GAS has a non-negligible enhancement effect on the formation rate of the SA–DMA binary nucleation system in view of its binding property and the estimated equilibrium concentration in the atmosphere.

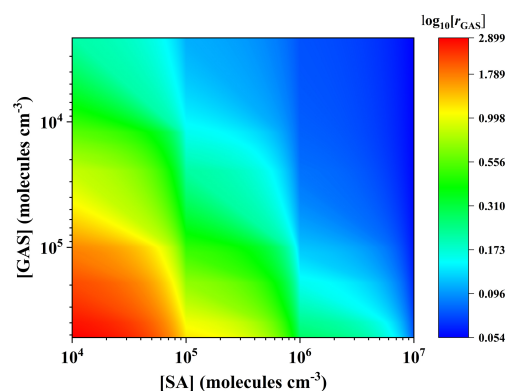


Figure 4. The cluster formation rate ratio (r_{GAS}) versus [SA] and [GAS] at $[\text{DMA}] = 10^8$ molec. cm^{-3} and 278 K. The color bars are values for $\log_{10}[r_{\text{GAS}}]$.

A series of kinetic simulations were further carried out by ACDC under different temperatures and [DMA] so as to achieve a deeper understanding of the enhancing potential of GAS. The influence of the varying temperature (258, 278 and 298 K) and [DMA] (10^7 , 10^8 and 10^9 molec. cm^{-3}) on the cluster formation rates is shown in Fig. 5. As shown in Fig. 5a, the increasing trends of $J_{\text{GAS-SA-DMA}}$ are similar at different temperatures, but $J_{\text{GAS-SA-DMA}}$ markedly increases and reaches 10^{-4} to 5 $\text{cm}^{-3} \text{s}^{-1}$ as the temperature changes from 298 to 258 K. The relatively low temperature can promote the cluster formation rate, probably due to its effect on the decrease in evaporation rates for the related clusters, because the low temperature inhibits the endothermic thermodynamic process of cluster evaporation to some extent. The $J_{\text{GAS-SA-DMA}}$ also tends to increase by 3 orders of magnitude with increasing [DMA] from 10^7 to 10^9 molec. cm^{-3} (Fig. 5b). This is possibly due to the fact that hydrogen bonding interaction increases between acidic molecules (GAS and SA) and the increased base molecules (DMA), which further results in the phenomenon of formation rate increase. These results demonstrate that the produced GAS from the chemical reaction of SO_3 with GA can speed up the SA–DMA nucleation even more dramatically under high [DMA] and at low temperature. This suggests that the enhancing potential of organosulfates in the SA–DMA-driven NPF deserves more attention in highly amine-polluted regions, especially with lower temperature, such as high mountains and cold polar areas.

3.5 Cluster growth pathways

Figure 6 presents the main growth pathways of the GAS–SA–DMA-based clusters at different [GAS] (10^4 – 10^6 molec. cm^{-3}) with an [SA] of 10^5 molec. cm^{-3} and a [DMA] of 10^8 molec. cm^{-3} at 278 K, traced employing ACDC. When [GAS] is 10^4 or 10^5 molec. cm^{-3} (Fig. 6a, b), the nucleation involves two primary pathways: (1) the pure

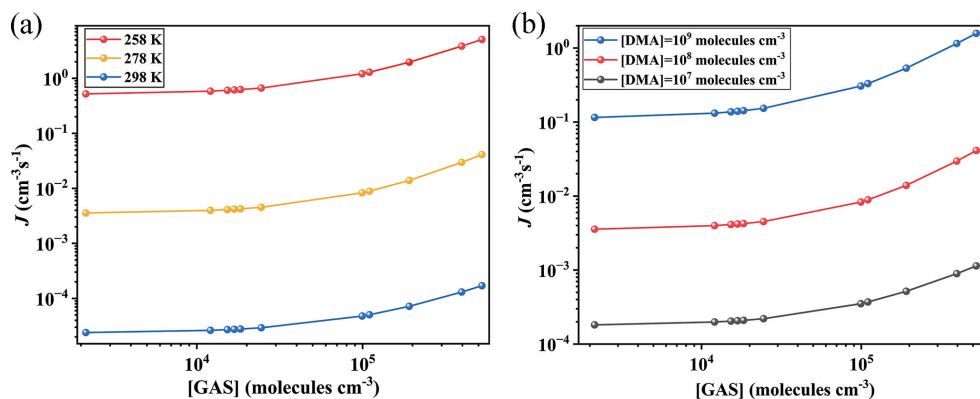


Figure 5. Simulated cluster formation rates $J_{\text{GAS-SA-DMA}}$ ($\text{cm}^{-3}\text{s}^{-1}$) (a) as a function of $[\text{GAS}]$ and temperature at $[\text{DMA}] = 10^8 \text{ molec. cm}^{-3}$ and $[\text{SA}] = 10^5 \text{ molec. cm}^{-3}$ and (b) as a function of $[\text{GAS}]$ and $[\text{DMA}]$ at 278 K and $[\text{SA}] = 10^5 \text{ molec. cm}^{-3}$.

SA–DMA nucleation pathway and (2) the GAS–SA–DMA nucleation pathway. In both pathways, the formation of the $(\text{SA})_1 \cdot (\text{DMA})_1$ cluster is the first step from monomers of SA and DMA. The pure SA–DMA cluster (black arrows) grows by the stepwise addition of either SA or DMA; i.e., each addition of an SA molecule is followed by one additional DMA molecule. In the case of the GAS–SA–DMA nucleation pathway (green arrows), the initially formed GAS-involved cluster is $(\text{GAS})_1 \cdot (\text{SA})_1 \cdot (\text{DMA})_1$, generated from GAS collision with the pre-existing $(\text{SA})_1 \cdot (\text{DMA})_1$ cluster. Then the $(\text{GAS})_1 \cdot (\text{SA})_1 \cdot (\text{DMA})_1$ cluster grows via a base-stabilization mechanism, which is similar to the pure SA–DMA nucleation pathway. The ternary cluster growth path follows the sequence $(\text{GAS})_1 \cdot (\text{SA})_1 \cdot (\text{DMA})_1 \rightarrow (\text{GAS})_1 \cdot (\text{SA})_1 \cdot (\text{DMA})_2 \rightarrow (\text{GAS})_1 \cdot (\text{SA})_2 \cdot (\text{DMA})_2 \rightarrow (\text{GAS})_1 \cdot (\text{SA})_2 \cdot (\text{DMA})_3 \rightarrow \text{flux-out}$. With the increase in $[\text{GAS}]$ to $10^6 \text{ molec. cm}^{-3}$ (Fig. 6c), another alternative GAS-involved pathway appears. Of particular note, the third growth pathway forms from the $(\text{GAS})_1 \cdot (\text{SA})_1 \cdot (\text{DMA})_2$ cluster. Thereafter, the cluster growth proceeds by adding one GAS monomer to the $(\text{GAS})_1 \cdot (\text{SA})_1 \cdot (\text{DMA})_2$ cluster, leading to the formation of the $(\text{GAS})_2 \cdot (\text{SA})_1 \cdot (\text{DMA})_2$ cluster. Then, the $(\text{GAS})_2 \cdot (\text{DMA})_2$ clusters flux out after the subsequent evaporation of the SA molecule. In this case, the contribution of GAS to the main cluster growth pathway increases from 3% (Fig. 6a) to 78% (73% + 5%) (Fig. 6c), with $[\text{GAS}]$ increasing from 10^4 to $10^6 \text{ molec. cm}^{-3}$. The GAS molecules do participate in the growth of clusters and further flux-out instead of evaporating from the existing clusters. Interestingly, in a previous study on methyl hydrogen sulfate (MHS) (Li et al., 2018; Liu et al., 2019), which is mainly produced from atmospheric chemical reactions, the reported cluster pathway of the MHS–SA–DMA system is very similar to that of the GAS–SA–DMA system we observed. Therefore, the cluster growth pathway of the GAS–SA–DMA system may represent a common feature for the mechanism of organosulfates participating in the SA–DMA-driven NPF.

The main growth pathways of the GA–SA–DMA system were also investigated and compared with that of the GAS–SA–DMA system (Fig. S10). By contrast, GA is not substantially conducive to the SA–DMA-based cluster growth, and the path only involves pure SA–DMA clusters at $[\text{GA}] = 10^9 \text{ molec. cm}^{-3}$ (Fig. S10b). Till $[\text{GA}]$ increases to $10^{10} \text{ molec. cm}^{-3}$ (Fig. S10c), and GA can indirectly participate in the cluster growth, acting as a “mediate bridge” and finally evaporating. This is consistent with the probed mediate bridge mechanism of the GA–SA– NH_3 system (Zhang et al., 2017). The GA molecule in the GA–SA–DMA system initially participates in the cluster growth and then evaporates from the newly formed clusters, mainly on account of the high evaporation rates of GA-containing clusters, which range from 20 to 10^6 s^{-1} for the $(\text{GA})_1(\text{SA})_2(\text{DMA})_3$, $(\text{GA})_2(\text{SA})_1(\text{DMA})_3$ and $(\text{GA})_3(\text{DMA})_3$ clusters. The growth pathways of the GAS–SA–DMA and GA–SA–DMA systems are obviously different. It can be concluded that GAS is an important “participator” rather than GA just as a mediate bridge when participating in the SA–DMA nucleation. This difference could mainly result from the higher stability of the $(\text{GAS})_1(\text{SA})_2(\text{DMA})_3$ and $(\text{GAS})_3(\text{DMA})_3$ clusters compared to those of the $(\text{GA})_1(\text{SA})_2(\text{DMA})_3$, $(\text{GA})_2(\text{SA})_1(\text{DMA})_3$ and $(\text{GA})_3(\text{DMA})_3$ clusters with high evaporation rates (in all cases larger than 10^1 s^{-1}) at the studied precursor concentrations (Figs. 2 and S7 and Table S6), with the GA-involved clusters evaporating into smaller clusters.

The cluster growth pathways of the GAS–SA–DMA system at different temperatures (258, 278 and 298 K) were also compared (Fig. S11). The proportion of the GAS-involved path increases with the decreasing temperature. At 258 K, the $(\text{SA})_2(\text{DMA})_2$ cluster can directly form the $(\text{GAS})_1(\text{SA})_2(\text{DMA})_2$ cluster through the addition of one GAS molecule. In that case, SA–DMA-based clusters can even assist the growth of clusters containing GAS from the 2 : 2 size, contributing to another growth pathway to

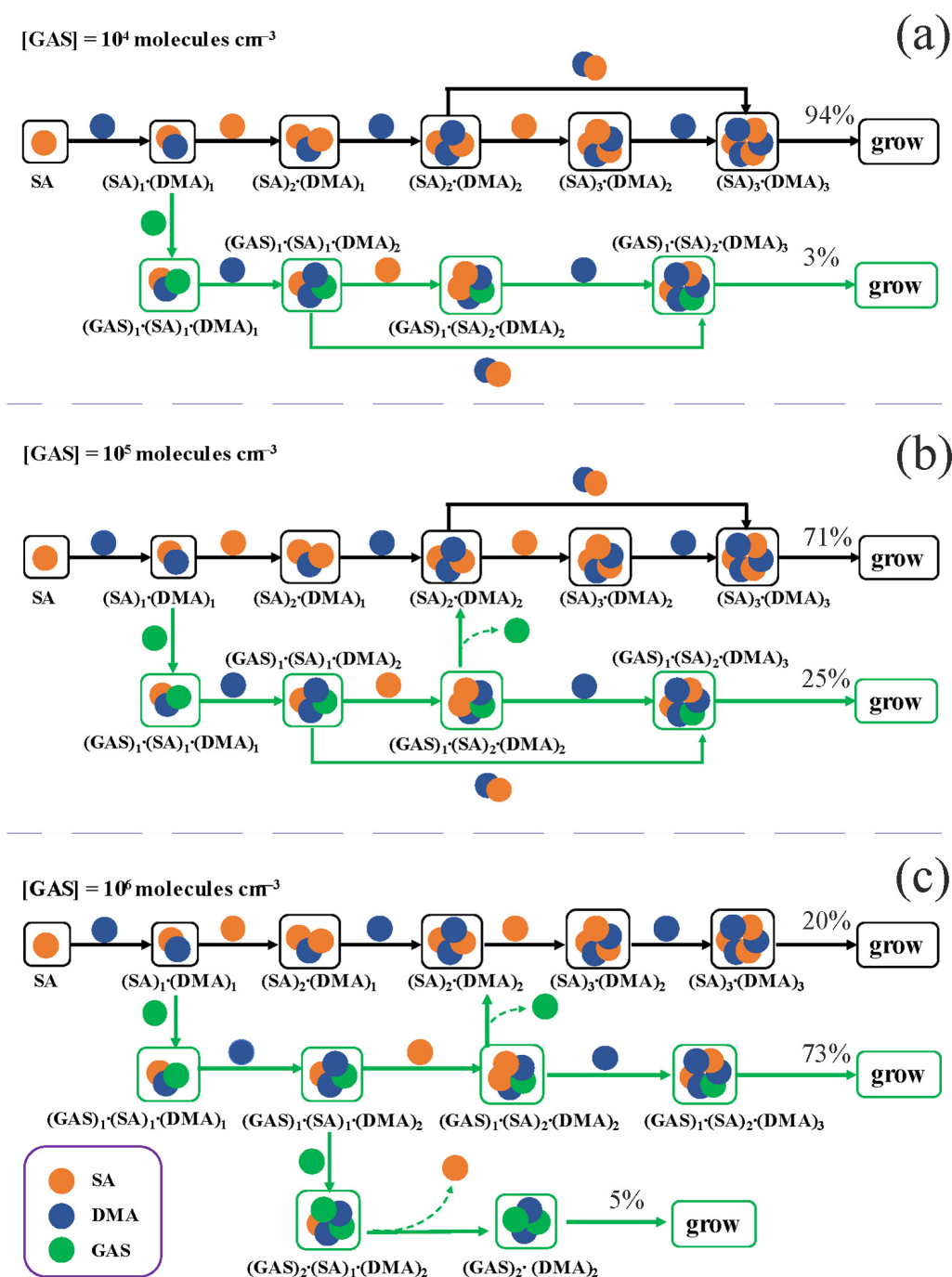


Figure 6. The main cluster growth pathway of the GAS–SA–DMA nucleation system at 278 K, $[DMA] = 10^8$, $[SA] = 10^5$ and (a) $[GAS] = 10^4$, (b) $[GAS] = 10^5$ and (c) $[GAS] = 10^6 \text{ molec. cm}^{-3}$. The black and green arrows refer to the pathways of SA–DMA and GAS–SA–DMA, respectively. For clarity, other pathways that contributes less than 5% to the cluster growing out of the studied system are not shown.

form large GAS-involved clusters. The founded alternative pathway emerges from the SA–DMA-based cluster to form $(GAS)_1 \cdot (SA)_2 \cdot (DMA)_2$, leading to the proportion of a GAS-involved path increase of up to 53%. This phenomenon may be because low temperature could efficiently promote

the thermodynamical stabilization of ternary clusters. Such a positive correlation of cluster stability with low temperature has also been suggested as a common feature in studies of other ternary systems containing acidic compounds, e.g.,

MSA, MSIA or NA (L. Liu et al., 2021b; Ning and Zhang, 2022; Ning et al., 2020).

3.6 Comparison with observations

Intense NPF events as well as emission of a suite of various nucleation precursors have been observed at the summit of Mt. Tai in China in recent years (Mochizuki et al., 2017; Lv et al., 2018). The gaseous concentration of GA reaches 343 ng m^{-3} during more field-burning-influenced periods at Mt. Tai (Mochizuki et al., 2017). The formation rates of 3 nm particles lie in the range of $0.82\text{--}25.04 \text{ cm}^{-3} \text{ s}^{-1}$ (Lv et al., 2018). The condensation sink (CS) (with an average of $1.4 \times 10^{-2} \text{ s}^{-1}$) and air temperature were found to be lower, whereas the concentration of SO_2 was higher on NPF days than that on non-NPF days. A strong correlation existed between the continental air mass passing through the polluted regions and NPF, which was partly because of the higher SO_2 concentration, indicating that SA was an important precursor on Mt. Tai. However, the pure SA–base nucleation could not fully explain the observed cluster formation rates (J_{obs}) attributed to the deficiency of the SA concentration. Given the fact that GA has only a slight influence on the nucleation and growth processes of atmospheric clusters, the reaction between GA and SO_3 may provide a secondary source of the potential precursor since high concentrations of sulfur oxides were detected. Interestingly, in this work, its product, GAS, was identified as having the ability to stabilize SA–DMA-based clusters and being able to speed up SA–DMA nucleation obviously. Hence, coupled with the published observational evidence at Mt. Tai in China (Mochizuki et al., 2017; Lv et al., 2018) and our aforementioned theoretical analysis, it can be supposed that these NPF events involve GAS.

In Fig. 7, we plotted the cluster formation rates for the pathways SA–DMA, GA–SA–DMA and GAS–SA–DMA, individually. Note that the calculated cluster formation rates via ACDC simulation in this work have a cluster size of about $\sim 1.3 \text{ nm}$. The observed cluster formation rates (J_3) at Mt. Tai were measured at 3 nm. According to the revised Kerminen–Kulmala equation (Anttila et al., 2010; Lehtinen et al., 2007), the cluster formation rate is $J_3 \approx 0.5 J_{1,3}$ (see the details in the Supplement). Hence, the $J_{3 \text{ nm}}(\text{SA–DMA})$, $J_{3 \text{ nm}}(\text{GA–SA–DMA})$ and $J_{3 \text{ nm}}(\text{GAS–SA–DMA})$ presented in Fig. 7 are calculated from 0.5 times their associated cluster formation rates ($J_{\text{SA–DMA}}$, $J_{\text{GA–SA–DMA}}$ and $J_{\text{GAS–SA–DMA}}$, respectively) obtained via the ACDC simulations. Here we can see that the needed concentration of SA for the binary SA–DMA (dotted lines) is clearly higher than those for the ternary GA–SA–DMA (dashed lines) and GAS–SA–DMA (solid lines) systems under the condition of the same formation rates. The needed [SA] for the GAS–SA–DMA system is obviously lower than that for GA–SA–DMA and markedly reduces with a [GAS] increase. In contrast, although [GA] is higher than [GAS] in Fig. 7, the variation of the needed [SA] for the

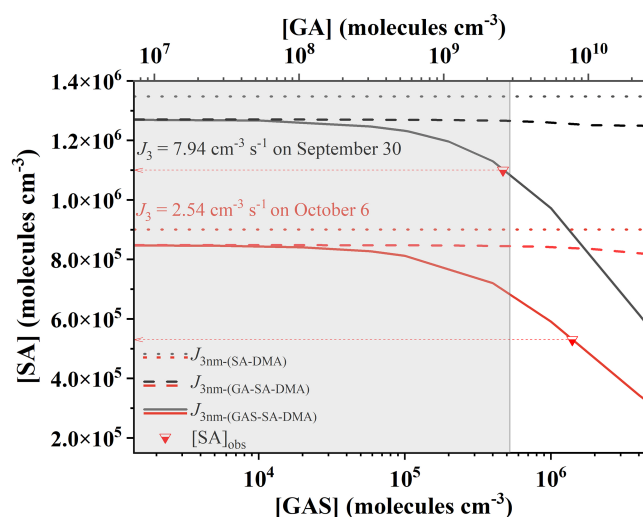


Figure 7. Required atmospheric concentrations of gas-phase precursors for the pathways SA–DMA, GA–SA–DMA and GAS–SA–DMA to reach the observed cluster formation rates (J_3) on 30 September 2014 (black lines) and 6 October 2014 (red lines) observed at Mt. Tai in China. [DMA] was set to $10^8 \text{ molec. cm}^{-3}$. Dotted red lines pointing from inverted triangles to arrows represent the observed [SA] on 30 September and 6 October 2014, respectively. The shaded area represents the globally observed [GA] and corresponding [GAS]. The simulated $J_{3 \text{ nm}}(\text{SA–DMA})$, $J_{3 \text{ nm}}(\text{GA–SA–DMA})$ and $J_{3 \text{ nm}}(\text{GAS–SA–DMA})$ are represented by dotted lines, dashed lines and solid lines, individually. The observation data of [GA] and the particle formation rates (J_3) come from Mochizuki et al. (2017) and Lv et al. (2018), respectively.

GA–SA–DMA system is minor with the increase in [GA]. These results imply that the influence of GAS on the SA–DMA system is stronger than that of GA, and the ternary GAS–SA–DMA mechanism provides a new pathway for the NPF events with the condition of relatively low [SA] observed at Mt. Tai. The shaded area shown in Fig. 7 represents the globally observed [GA] as well as the corresponding [GAS]. The [SA] at Mt. Tai on 30 September 2014 is observed at $1.09 \times 10^6 \text{ molec. cm}^{-3}$ (the top red line pointing from an inverted triangle to the left arrow). If the new particles at Mt. Tai on 30 September 2014 are presumed to be produced from the pure SA–DMA system with the typical [DMA] of $10^8 \text{ molec. cm}^{-3}$, the concentration of SA around $\sim 1.35 \times 10^6 \text{ molec. cm}^{-3}$ is needed (the black dotted line), which is a bit higher than the observed [SA]. To reach the observed $J_{30 \text{ September}}$ ($7.94 \text{ cm}^{-3} \text{ s}^{-1}$), the required [GAS] relevant to the observed [SA] on 30 September 2014 is $\sim 4.70 \times 10^5 \text{ molec. cm}^{-3}$ in the shaded area as shown in Fig. 7. This indicates that the ternary GAS–SA–DMA nucleation mechanism corresponds well to the observed records of the [SA] and NPF events. As for the GA–SA–DMA pathway, the required [GA] and [SA] are presented by black and red dashed lines. It is very clear that the GA–SA–DMA ternary system is not sufficient enough to unravel the observed NPF

at Mt. Tai, for which the [GA] corresponding to the observed [SA] is beyond the boundary of the shaded area. In another example, if the new particles on 6 October 2014 are assumed to be generated from the pure SA–DMA system, the required [SA] is estimated to be $\sim 9.01 \times 10^5 \text{ molec. cm}^{-3}$ (the red dotted line), which is also too high for the observed [SA] ($5.3 \times 10^5 \text{ molec. cm}^{-3}$, the bottom red line pointing from the inverted triangle to the left arrow). Although GAS can speed up the SA–DMA-driven NPF (the red line), to reach the observed $J_{6 \text{ October}}$ ($2.54 \text{ cm}^{-3} \text{ s}^{-1}$), a fairly high concentration of GAS is required, which is outside the shaded area. This suggests that there may be other potential enhanced mechanisms for atmospheric new particle formation, which require more in-depth studies. These results and analyses suggest that the GAS–SA–DMA nucleation mechanism can explain the field observation of the atmospheric SA-involved particles at Mt. Tai, while the binary SA–DMA nucleation is incompatible with the observed new particle formation rates. Therefore, it can be concluded that the GAS produced from the chemical reaction of GA and SO_3 could play an important role in speeding up the SA–DMA-driven NPF events at Mt. Tai. In the light of the deficiency of field observations of GAS in the gas phase, further detection of GAS is still needed.

4 Atmospheric implications

This study reveals that the reaction of GA and SO_3 can generate a certain concentration of GAS as a potential atmospheric nucleation precursor, and the GAS is able to intensely speed up the SA–DMA nucleation. Therefore, GA in the atmosphere can consume part of SO_3 , which may lead to the observed relatively low SA concentration, but its product GAS can significantly enhance the SA–DMA-driven NPF under such conditions. Considering the high-atmospheric gas-phase concentrations of GA and particle-phase GAS detected in diverse environments in regions worldwide, including Finnish forest, German rural, Japanese forest and the marine atmosphere of the North Pacific (Ehn et al., 2010; Miyazaki et al., 2014; Mochizuki et al., 2017, 2019; Stieger et al., 2021), GAS could be an important contributor to SA–DMA-driven NPF in locations with a high GA concentration and a relatively low SA concentration. To further evaluate the implication of GAS for the SA–DMA nucleation in the atmosphere, the specific contribution of the SA–DMA cluster growth paths with or without GAS to NPF was calculated under the ambient conditions in the corresponding regions (Fig. 8). The branch ratios of the major flux-out were investigated under varying [GAS] (1.21×10^4 – $5.24 \times 10^5 \text{ molec. cm}^{-3}$) and [SA] (3×10^4 – $5.20 \times 10^5 \text{ molec. cm}^{-3}$) at 278 K, which were basically from the field observations, including Mt. Tai (36.26° N , 117.11° E), Sapporo ($42^\circ 59' \text{ N}$, $141^\circ 23' \text{ E}$), Melpitz ($51^\circ 32' \text{ N}$, $12^\circ 56' \text{ E}$), Hyytiälä ($61^\circ 51' \text{ N}$, $24^\circ 17' \text{ E}$), Ho-

henpeissenberg ($47^\circ 48' \text{ N}$, $11^\circ 00' \text{ E}$) and the subarctic North Pacific (Stieger et al., 2021; Mochizuki et al., 2017, 2019; Miyazaki et al., 2014; Mikkonen et al., 2011). The concentrations of GAS or SA recorded in green as well as that of DMA are set to be a median in this study ($1 \times 10^5 \text{ molec. cm}^{-3}$ for [SA], $1.28 \times 10^5 \text{ molec. cm}^{-3}$ for [GAS] and $1 \times 10^8 \text{ molec. cm}^{-3}$ for [DMA]). As presented in Fig. 8, the branch ratio of the flux-out is very sensitive to the [GAS]. In the high-[GAS] regions, such as Melpitz ($3.96 \times 10^5 \text{ molec. cm}^{-3}$) and Mt. Tai ($5.24 \times 10^5 \text{ molec. cm}^{-3}$), the contributions of the GAS–SA–DMA growth pathways (red pie in Fig. 8) are dominant in their NPF. For regions with relatively low [GAS], e.g., Sapporo and subarctic North Pacific, the contributions of GAS-involved clustering pathways are 12 % and 16 %, respectively. Especially in the region with low SA abundance, like Hyytiälä, the nucleation was also identified as being dominated by the GAS–SA–DMA path, resulting in around 80 % of the cluster formation. This implies that the influence of GAS in regions with relatively low SA concentrations is also prominent. Note that the GAS concentrations we discussed in this work are estimated from limited observational data of SO_3 and GA in the atmosphere. The actual atmospheric concentration of GAS still requires a large number of field observations to achieve more in-depth research.

This study found that low temperatures and high DMA concentrations are both favorable conditions for the higher enhancing potential of GAS in the SA–DMA nucleation. Therefore, in cold areas, the contribution of GAS to NPF deserves more attention, especially under the polluted conditions of high DMA abundance. The identified nucleation mechanism of the GAS–SA–DMA system, in which GAS playing a participator role can not only promote the initial nucleation but also participate in the subsequent nucleation processes, also provides a feasible potential source of organosulfate in aerosol. When ignoring the contribution of organosulfate produced from the chemical reaction with the NPF, the risk of hydroxy acid emissions and the sources of organic aerosols may be underestimated to some extent. Recently, more and more field observation data of hydroxy acids in diverse environments worldwide have been reported (Chen et al., 2021; Mochizuki et al., 2016; Duncan et al., 2019). The identified reaction mechanism in this study appears to be generalizable to evaluate the role of these acids, such as lactic acid and their derivatives in atmospheric NPF. To the best of the authors' knowledge, the roles of hydroxy acids as well as their derivatives in atmospheric NPFs have not been systematically reported before. The current findings imply the necessity of further studying the NPFs affected via chemical reactions of organic acids in the atmosphere. Including this new organosulfate chemistry in the existing atmospheric models will improve the quantitative modeling of the effect of organic acids on atmospheric aerosol formation. Lastly, organosulfates produced from secondary sources, like gas-

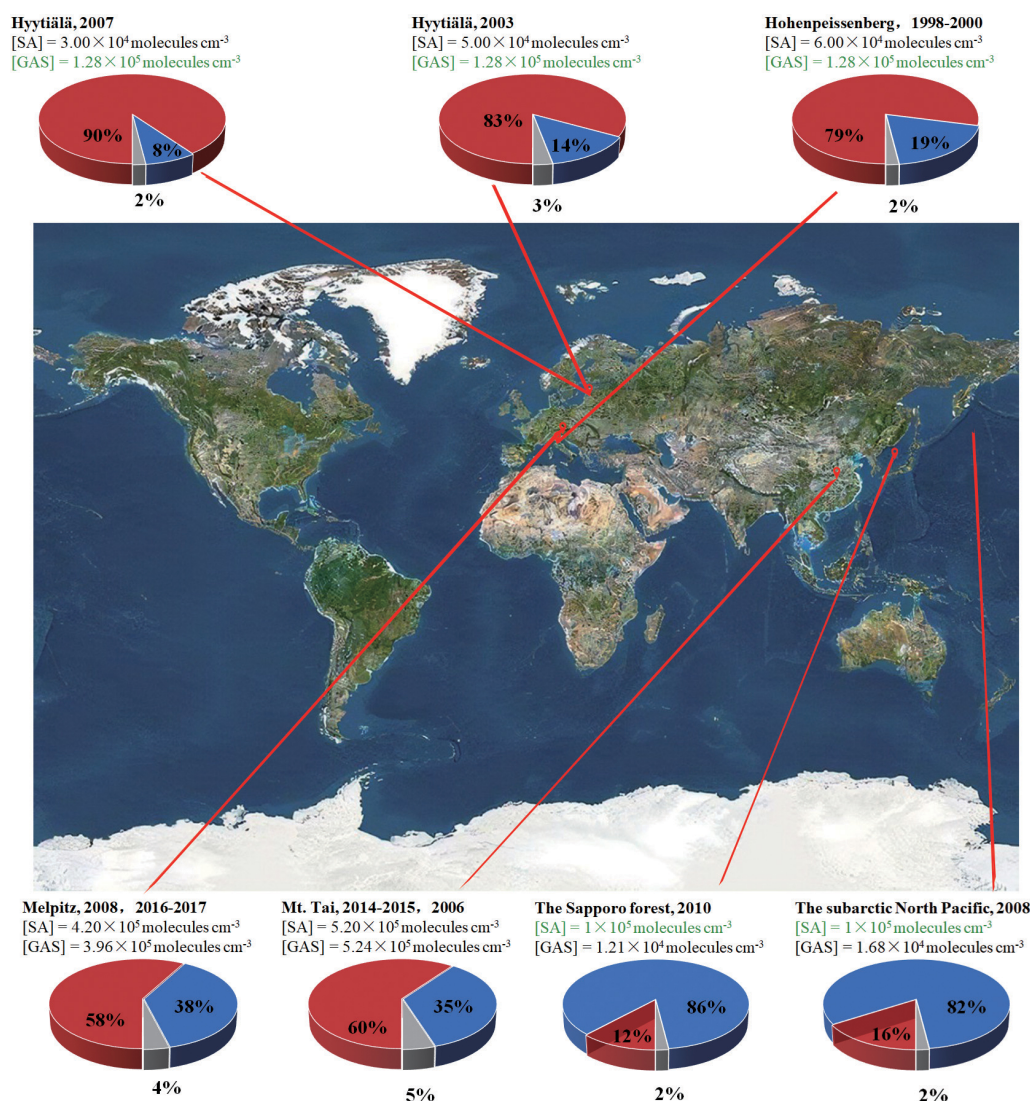


Figure 8. The branch ratio of the GAS–SA–DMA (red pie) and SA–DMA (blue pie) growth pathways based on field data in different regions with a different [GAS]. The data recorded in black are from field observations, and those in green are set to be a median in this study. [DMA] = 10^8 molec. cm⁻³. The map is from © Google Maps (<https://www.google.com/maps>, last access: 22 November 2022).

phase chemical reactions, are deserving of further monitoring and evaluating.

Data availability. Data from this research are not publicly available. Interested researchers can contact the corresponding author of this article.

Supplement. Computational details are available for the concentration of GAS as well as GASA, judging from the GA–SA–DMA, GAS–SA–DMA and GASA–SA–DMA cluster stability and boundary conditions, variable settings of ACDC, the catalytic effect of GA on SO₃–H₂O reaction, conformations of the GA–SA–DMA and GAS–SA–DMA clusters and GASA–SA–DMA clusters, evaporation coefficients for all the evaporation pathways of the clusters

investigated in this work, the effect of [SA] on the GA–SA–DMA and GAS–SA–DMA clusters and the GASA–SA–DMA cluster formation rates, the main cluster growth pathways of the GAS–SA–DMA system in comparison with that of the GA–SA–DMA system, and details for the thermodynamic information on the formation of the GA–SA–DMA, GAS–SA–DMA and GASA–SA–DMA clusters. The supplement related to this article is available online at: <https://doi.org/10.5194/acp-24-3593-2024-supplement>.

Author contributions. Conceptualization of the research goals, development of the methodology and construction of the models were completed by XZ and ST under the supervision of SY. YL assisted in the data analyses. XZ prepared the original draft, which was subsequently reviewed and edited by all the co-authors.

Competing interests. The contact author has declared that none of the authors has any competing interests.

Disclaimer. Publisher's note: Copernicus Publications remains neutral with regard to jurisdictional claims made in the text, published maps, institutional affiliations, or any other geographical representation in this paper. While Copernicus Publications makes every effort to include appropriate place names, the final responsibility lies with the authors.

Acknowledgements. The authors acknowledge the financial support of the National Natural Science Foundation of China and the GuangDong Basic and Applied Basic Research Foundation.

Financial support. This research has been supported by the National Natural Science Foundation of China (grant no. 21976061) and the Basic and Applied Basic Research Foundation of Guangdong Province (grant nos. 2022A1515010591 and 2024A1515011470).

Review statement. This paper was edited by Jason Surratt and reviewed by two anonymous referees.

References

- Almeida, J., Schobesberger, S., Kurten, A., Ortega, I. K., Kupiainen-Maatta, O., Praplan, A. P., Adamov, A., Amorim, A., Bianchi, F., Breitenlechner, M., David, A., Dommen, J., Donahue, N. M., Downard, A., Dunne, E., Duplissy, J., Ehrhart, S., Flagan, R. C., Franchin, A., Guida, R., Hakala, J., Hansel, A., Heinritzi, M., Henschel, H., Jokinen, T., Junninen, H., Kajos, M., Kangasluoma, J., Keskinen, H., Kupc, A., Kurten, T., Kvashin, A. N., Laaksonen, A., Lehtipalo, K., Leiminger, M., Leppa, J., Loukonen, V., Makhmutov, V., Mathot, S., McGrath, M. J., Nieminen, T., Olenius, T., Onnela, A., Petaja, T., Riccobono, F., Riipinen, I., Rissanen, M., Rondo, L., Ruuskanen, T., Santos, F. D., Sarnela, N., Schallhart, S., Schnitzhofer, R., Seinfeld, J. H., Simon, M., Sipila, M., Stozhkov, Y., Stratmann, F., Tome, A., Trostl, J., Tsagkogeorgas, G., Vaattovaara, P., Viisanen, Y., Virtanen, A., Vrtala, A., Wagner, P. E., Weingartner, E., Wex, H., Williamson, C., Wimmer, D., Ye, P. L., Yli-Juuti, T., Carslaw, K. S., Kulmala, M., Curtius, J., Baltensperger, U., Worsnop, D. R., Vehkamäki, H., and Kirkby, J.: Molecular Understanding of Sulphuric Acid-Amine Particle Nucleation in the Atmosphere, *Nature*, 502, 359–363, <https://doi.org/10.1038/nature12663>, 2013.
- Anttila, T., Kerminen, V.-M., and Lehtinen, K. E. J.: Parameterizing the formation rate of new particles: The effect of nuclei self-coagulation, *J. Aerosol Sci.*, 41, 621–636, <https://doi.org/10.1016/j.jaerosci.2010.04.008>, 2010.
- Birmili, W., Berresheim, H., Plass-Dülmer, C., Elste, T., Gilge, S., Wiedensohler, A., and Uhrner, U.: The Hohenpeissenberg aerosol formation experiment (HAFEX): a long-term study including size-resolved aerosol, H₂SO₄, OH, and monoterpenes measurements, *Atmos. Chem. Phys.*, 3, 361–376, <https://doi.org/10.5194/acp-3-361-2003>, 2003.
- Brüggemann, M., Poulain, L., Held, A., Stelzer, T., Zuth, C., Richters, S., Mutzel, A., van Pinxteren, D., Iinuma, Y., Katkevica, S., Rabe, R., Herrmann, H., and Hoffmann, T.: Real-time detection of highly oxidized organosulfates and BSOA marker compounds during the F-BEACH 2014 field study, *Atmos. Chem. Phys.*, 17, 1453–1469, <https://doi.org/10.5194/acp-17-1453-2017>, 2017.
- Brüggemann, M., Xu, R., Tilgner, A., Kwong, K. C., Mutzel, A., Poon, H. Y., Otto, T., Schaefer, T., Poulain, L., Chan, M. N., and Herrmann, H.: Organosulfates in Ambient Aerosol: State of Knowledge and Future Research Directions on Formation, Abundance, Fate, and Importance, *Environ. Sci. Technol.*, 54, 3767–3782, <https://doi.org/10.1021/acs.est.9b06751>, 2020.
- Cao, Y., Zhou, H., Jiang, W., Chen, C.-W., and Pan, W.-P.: Studies of the Fate of Sulfur Trioxide in Coal-Fired Utility Boilers Based on Modified Selected Condensation Methods, *Environ. Sci. Technol.*, 44, 3429–3434, <https://doi.org/10.1021/es903661b>, 2010.
- Chen, D., Li, D., Wang, C., Liu, F., and Wang, W.: Formation Mechanism of Methanesulfonic Acid and Ammonia Clusters: A Kinetics Simulation Study, *Atmos. Environ.*, 222, 117161, <https://doi.org/10.1016/j.atmosenv.2019.117161>, 2020.
- Chen, L. and Bhattacharya, S.: Sulfur emission from Victorian brown coal under pyrolysis, oxy-fuel combustion and gasification conditions, *Environ. Sci. Technol.*, 47, 1729–1734, <https://doi.org/10.1021/es303364g>, 2013.
- Chen, Y., Guo, H., Nah, T., Tanner, D. J., Sullivan, A. P., Takeuchi, M., Gao, Z., Vasilakos, P., Russell, A. G., Baumann, K., Huey, L. G., Weber, R. J., and Ng, N. L.: Low-Molecular-Weight Carboxylic Acids in the Southeastern U.S.: Formation, Partitioning, and Implications for Organic Aerosol Aging, *Environ. Sci. Technol.*, 55, 6688–6699, <https://doi.org/10.1021/acs.est.1c01413>, 2021.
- Clark, T., Chandrasekhar, J., Spitznagel, G. W., and Schleyer, P. V. R.: Efficient diffuse function-augmented basis sets for anion calculations. III. The 3-21+G basis set for first-row elements, Li–F, *J. Comput. Chem.*, 4, 294–301, <https://doi.org/10.1002/jcc.540040303>, 1983.
- Dal Maso, M., Sogacheva, L., Aalto, P. P., Riipinen, I., Kompula, M., Tunved, P., Korhonen, L., Suur-Uski, V., Hirsikko, A., Kurtén, T., Kerminen, V.-M., Lihavainen, H., Viisanen, Y., Hansson, H.-C., and Kulmala, M.: Aerosol size distribution measurements at four Nordic field stations: identification, analysis and trajectory analysis of new particle formation bursts, *Tellus B*, 59, 350–361, <https://doi.org/10.1111/j.1600-0889.2007.00267.x>, 2007.
- Dal Maso, M., Hyvärinen, A., Komppula, M., Tunved, P., Kerminen, V.-M., Lihavainen, H., Öviisanen, Y., Hansson, H.-C., and Kulmala, M.: Annual and interannual variation in boreal forest aerosol particle number and volume concentration and their connection to particle formation, *Tellus B*, 60, 495–508, <https://doi.org/10.1111/j.1600-0889.2008.00366.x>, 2008.
- Darer, A. I., Cole-Filipiak, N. C., O'Connor, A. E., and Elrod, M. J.: Formation and Stability of Atmospherically Relevant Isoprene-Derived Organosulfates and Organonitrates, *Environ. Sci. Technol.*, 45, 1895–1902, <https://doi.org/10.1021/es103797z>, 2011.
- Duncan, S. M., Tomaz, S., Morrison, G., Webb, M., Atkin, J., Surratt, J. D., and Turpin, B. J.: Dynamics of Res-

- idential Water-Soluble Organic Gases: Insights into Sources and Sinks, *Environ. Sci. Technol.*, 53, 1812–1821, <https://doi.org/10.1021/acs.est.8b05852>, 2019.
- Ehn, M., Junninen, H., Petäjä, T., Kurtén, T., Kerminen, V.-M., Schobesberger, S., Manninen, H. E., Ortega, I. K., Vehkamäki, H., Kulmala, M., and Worsnop, D. R.: Composition and temporal behavior of ambient ions in the boreal forest, *Atmos. Chem. Phys.*, 10, 8513–8530, <https://doi.org/10.5194/acp-10-8513-2010>, 2010.
- Ehn, M., Thornton, J. A., Kleist, E., Sipilä, M., Junninen, H., Pullinen, I., Springer, M., Rubach, F., Tillmann, R., and Lee, B.: A large source of low-volatility secondary organic aerosol, *Nature*, 506, 476–479, <https://doi.org/10.1038/nature13032>, 2014.
- Elm, J., Bilde, M., and Mikkelsen, K. V.: Assessment of Density Functional Theory in Predicting Structures and Free Energies of Reaction of Atmospheric Prenucleation Clusters, *J. Chem. Theory Comput.*, 8, 2071–2077, <https://doi.org/10.1021/ct300192p>, 2012.
- Elm, J., Myllys, N., Hyttinen, N., and Kurtén, T.: Computational Study of the Clustering of a Cyclohexene Autoxidation Product C₆H₈O₇ with Itself and Sulfuric Acid, *J. Phys. Chem. A*, 119, 8414–8421, <https://doi.org/10.1021/acs.jpca.5b04040>, 2015.
- Elm, J., Jen, C. N., Kurtén, T., and Vehkamäki, H.: Strong hydrogen bonded molecular interactions between atmospheric diamines and sulfuric acid, *J. Phys. Chem. A*, 120, 3693–3700, <https://doi.org/10.1021/acs.jpca.6b03192>, 2016.
- Feketeová, L., Bertier, P., Salbaing, T., Azuma, T., Calvo, F., Farizon, B., Farizon, M., and Märk, T. D.: Impact of a hydrophobic ion on the early stage of atmospheric aerosol formation, *P. Natl. Acad. Sci. USA*, 116, 22540–22544, <https://doi.org/10.1073/pnas.1911136116>, 2019.
- Frisch, M. J., Trucks, G. W., Schlegel, H. B., Scuseria, G. E., Robb, M. A., Cheeseman, J. R., Scalmani, G., Barone, V., Mennucci, B., Petersson, G. A., Nakatsuji, H., Caricato, M., Li, X., Hratchian, H. P., Izmaylov, A. F., Bloino, J., Zheng, G., Sonnenberg, J. L., Hada, M., Ehara, M., Toyota, K., Fukuda, R., Hasegawa, J., Ishida, M., Nakajima, T., Honda, Y., Kitao, O., Nakai, H., Vreven, T., Montgomery Jr., J. A., Peralta, J. E., Ogliaro, F., Bearpark, M., Heyd, J. J., Brothers, E., Kudin, K. N., Staroverov, V. N., Kobayashi, R., Normand, J., Raghavachari, K., Rendell, A., Burant, J. C., Iyengar, S. S., Tomasi, J., Cossi, M., Rega, N., Millam, J. M., Klene, M., Knox, J. E., Cross, J. B., Bakken, V., Adamo, C., Jaramillo, J., Gomperts, R., Stratmann, R. E., Yazyev, O., Austin, A. J., Cammi, R., Pomelli, C., Ochterski, J. W., Martin, R. L., Morokuma, K., Zakrzewski, V. G., Voth, G. A., Salvador, P., Dannenberg, J. J., Dapprich, S., Daniels, A. D., Farkas, O., Foresman, J. B., Ortiz, J. V., Cioslowski, J., and Fox, D. J.: Gaussian 09, Revision A.02, Gaussian, Inc., Wallingford, CT, 2009.
- Froyd, K. D., Murphy, S. M., Murphy, D. M., de Gouw, J. A., Eddingsaas, N. C., and Wennberg, P. O.: Contribution of isoprene-derived organosulfates to free tropospheric aerosol mass, *P. Natl. Acad. Sci. USA*, 107, 21360, <https://doi.org/10.1073/pnas.1012561107>, 2010.
- Ge, P., Luo, G., Luo, Y., Huang, W., Xie, H. B., and Chen, J. W.: A molecular-scale study on the hydration of sulfuric acid-amide complexes and the atmospheric implication, *Chemosphere*, 213, 453–462, <https://doi.org/10.1016/j.chemosphere.2018.09.068>, 2018a.
- Ge, P., Luo, G., Luo, Y., Huang, W., Xie, H. B., Chen, J. W., and Qu, J. P.: Molecular understanding of the interaction of amino acids with sulfuric acid in the presence of water and the atmospheric implication, *Chemosphere*, 210, 215–223, <https://doi.org/10.1016/j.chemosphere.2018.07.014>, 2018b.
- Ge, X. L., Wexler, A. S., and Clegg, S. L.: Atmospheric amines – Part I. A review, *Atmos. Environ.*, 45, 524–546, <https://doi.org/10.1016/j.atmosenv.2010.10.012>, 2011.
- Glasius, M., Hansen, A. M. K., Claeys, M., Henzing, J. S., Jedynska, A. D., Kasper-Giebl, A., Kistler, M., Kristensen, K., Martinsson, J., Maenhaut, W., Nøjgaard, J. K., Spindler, G., Stenström, K. E., Swietlicki, E., Szidat, S., Simpson, D., and Yttri, K. E.: Composition and sources of carbonaceous aerosols in Northern Europe during winter, *Atmos. Environ.*, 173, 127–141, <https://doi.org/10.1016/j.atmosenv.2017.11.005>, 2018.
- Hazra, M. K. and Sinha, A.: Formic Acid Catalyzed Hydrolysis of SO₃ in the Gas Phase: A Barrierless Mechanism for Sulfuric Acid Production of Potential Atmospheric Importance, *J. Am. Chem. Soc.*, 133, 17444–17453, <https://doi.org/10.1021/ja207393v>, 2011.
- Herb, J., Nadykto, A. B., and Yu, F.: Large ternary hydrogen-bonded pre-nucleation clusters in the Earth's atmosphere, *Chem. Phys. Lett.*, 518, 7–14, <https://doi.org/10.1016/j.cplett.2011.10.035>, 2011.
- Hettiyadura, A. P. S., Stone, E. A., Kundu, S., Baker, Z., Geddes, E., Richards, K., and Humphry, T.: Determination of atmospheric organosulfates using HILIC chromatography with MS detection, *Atmos. Meas. Tech.*, 8, 2347–2358, <https://doi.org/10.5194/amt-8-2347-2015>, 2015.
- Hettiyadura, A. P. S., Jayarathne, T., Baumann, K., Goldstein, A. H., de Gouw, J. A., Koss, A., Keutsch, F. N., Skog, K., and Stone, E. A.: Qualitative and quantitative analysis of atmospheric organosulfates in Centreville, Alabama, *Atmos. Chem. Phys.*, 17, 1343–1359, <https://doi.org/10.5194/acp-17-1343-2017>, 2017.
- Hirvonen, V., Myllys, N., Kurtén, T., and Elm, J.: Closed-Shell Organic Compounds Might Form Dimers at the Surface of Molecular Clusters, *J. Phys. Chem. A*, 122, 1771–1780, <https://doi.org/10.1021/acs.jpca.7b11970>, 2018.
- Huang, H.-L., Chao, W., and Lin, J. J.-M.: Kinetics of a Criegee intermediate that would survive high humidity and may oxidize atmospheric SO₂, *P. Natl. Acad. Sci. USA*, 112, 10857–10862, <https://doi.org/10.1073/pnas.1513149112>, 2015.
- Jen, C. N., McMurry, P. H., and Hanson, D. R.: Stabilization of sulfuric acid dimers by ammonia, methylamine, dimethylamine, and trimethylamine, *J. Geophys. Res.-Atmos.*, 119, 7502–7514, <https://doi.org/10.1002/2014JD021592>, 2014.
- Jimenez, J. L., Canagaratna, M. R., Donahue, N. M., Prevot, A. S. H., Zhang, Q., Kroll, J. H., DeCarlo, P. F., Allan, J. D., Coe, H., Ng, N. L., Aiken, A. C., Docherty, K. S., Ulbrich, I. M., Grieshop, A. P., Robinson, A. L., Duplissy, J., Smith, J. D., Wilson, K. R., Lanz, V. A., Hueglin, C., Sun, Y. L., Tian, J., Laaksonen, A., Raatikainen, T., Rautiainen, J., Vaattovaara, P., Ehn, M., Kulmala, M., Tomlinson, J. M., Collins, D. R., Cubison, M. J., Dunlea, E. J., Huffman, J. A., Onasch, T. B., Alfarra, M. R., Williams, P. I., Bower, K., Kondo, Y., Schneider, J., Drewnick, F., Borrmann, S., Weimer, S., Demerjian, K., Salcedo, D., Cottrell, L., Griffin, R., Takami, A., Miyoshi, T., Hatakeyama, S., Shimojo, A., Sun, J. Y., Zhang, Y. M., Dzepina, K., Kimmel, J. R., Sueper, D., Jayne, J. T., Herndon, S. C., Trimborn, A.

- M., Williams, L. R., Wood, E. C., Middlebrook, A. M., Kolb, C. E., Baltensperger, U., and Worsnop, D. R.: Evolution of Organic Aerosols in the Atmosphere, *Science*, 326, 1525–1529, <https://doi.org/10.1126/science.1180353>, 2009.
- Katz, D. J., Abdelhamid, A., Stark, H., Canagaratna, M. R., Worsnop, D. R., and Browne, E. C.: Chemical identification of new particle formation and growth precursors through positive matrix factorization of ambient ion measurements, *Atmos. Chem. Phys.*, 23, 5567–5585, <https://doi.org/10.5194/acp-23-5567-2023>, 2023.
- Kawamura, K. and Bikkina, S.: A review of dicarboxylic acids and related compounds in atmospheric aerosols: Molecular distributions, sources and transformation, *Atom. Res.*, 170, 140–160, <https://doi.org/10.1016/j.atmosres.2015.11.018>, 2016.
- Kirkby, J., Curtius, J., Almeida, J., Dunne, E., Duplissy, J., Ehrhart, S., Franchin, A., Gagne, S., Ickes, L., Kurten, A., Kupc, A., Metzger, A., Riccobono, F., Rondo, L., Schobesberger, S., Tsagkogeorgas, G., Wimmer, D., Amorim, A., Bianchi, F., Breitenlechner, M., David, A., Dommen, J., Downard, A., Ehn, M., Flagan, R. C., Haider, S., Hansel, A., Hauser, D., Jud, W., Junninen, H., Kreissl, F., Kvashin, A., Laaksonen, A., Lehtipalo, K., Lima, J., Lovejoy, E. R., Makhmutov, V., Mathot, S., Mikkilä, J., Minginette, P., Mogo, S., Nieminen, T., Onnela, A., Pereira, P., Petaja, T., Schnitzhofer, R., Seinfeld, J. H., Sipila, M., Stozhkov, Y., Stratmann, F., Tome, A., Vanhanen, J., Viisanen, Y., Vrtala, A., Wagner, P. E., Walther, H., Weingartner, E., Wex, H., Winkler, P. M., Carslaw, K. S., Worsnop, D. R., Baltensperger, U., and Kulmala, M.: Role of sulphuric acid, ammonia and galactic cosmic rays in atmospheric aerosol nucleation, *Nature*, 476, 429–433, <https://doi.org/10.1038/nature10343>, 2011.
- Kirkby, J., Duplissy, J., Sengupta, K., Frege, C., Gordon, H., Williamson, C., Heinritzi, M., Simon, M., Yan, C., Almeida, J., Trostl, J., Nieminen, T., Ortega, I. K., Wagner, R., Adamov, A., Amorim, A., Bernhammer, A. K., Bianchi, F., Breitenlechner, M., Brilke, S., Chen, X. M., Craven, J., Dias, A., Ehrhart, S., Flagan, R. C., Franchin, A., Fuchs, C., Guida, R., Hakala, J., Hoyle, C. R., Jokinen, T., Junninen, H., Kangasluoma, J., Kim, J., Krapf, M., Kurten, A., Laaksonen, A., Lehtipalo, K., Makhmutov, V., Mathot, S., Molteni, U., Onnela, A., Perakyla, O., Piel, F., Petaja, T., Praplan, A. P., Pringle, K., Rap, A., Richards, N. A. D., Riipinen, I., Rissanen, M. P., Rondo, L., Sarnela, N., Schobesberger, S., Scott, C. E., Seinfeld, J. H., Sipila, M., Steiner, G., Stozhkov, Y., Stratmann, F., Tome, A., Virtanen, A., Vogel, A. L., Wagner, A. C., Wagner, P. E., Weingartner, E., Wimmer, D., Winkler, P. M., Ye, P. L., Zhang, X., Hansel, A., Dommen, J., Donahue, N. M., Worsnop, D. R., Baltensperger, U., Kulmala, M., Carslaw, K. S., and Curtius, J.: Ion-induced nucleation of pure biogenic particles, *Nature*, 533, 521–526, <https://doi.org/10.1038/nature17953>, 2016.
- Kundu, S., Quraishi, T. A., Yu, G., Suarez, C., Keutsch, F. N., and Stone, E. A.: Evidence and quantitation of aromatic organosulfates in ambient aerosols in Lahore, Pakistan, *Atmos. Chem. Phys.*, 13, 4865–4875, <https://doi.org/10.5194/acp-13-4865-2013>, 2013.
- Kürten, A., Jokinen, T., Simon, M., Sipilä, M., Sarnela, N., Junninen, H., Adamov, A., Almeida, J., Amorim, A., Bianchi, F., Breitenlechner, M., Dommen, J., Donahue, N. M., Duplissy, J., Ehrhart, S., Flagan, R. C., Franchin, A., Hakala, J., Hansel, A., Heinritzi, M., Hutterli, M., Kangasluoma, J., Kirkby, J., Laaksonen, A., Lehtipalo, K., Leiminger, M., Makhmutov, V., Mathot, S., Onnela, A., Petäjä, T., Praplan, A. P., Riccobono, F., Rissanen, M. P., Ruuskanen, T., Santos, F. D., Schallhart, S., Schnitzhofer, R., Simon, M., Smith, J. N., Tröstl, J., Tsagkogeorgas, G., Tomé, A., Vaattovaara, P., Vehkamäki, H., Vrtala, A. E., Wagner, P. E., Williamson, C., Wimmer, D., Winkler, P. M., Virtanen, A., Donahue, N. M., Carslaw, K. S., Baltensperger, U., Riipinen, I., Curtius, J., Worsnop, D. R., and Kulmala, M.: The effect of acid–base clustering and ions on the growth of atmospheric nano-particles, *Nat. Commun.*, 7, 11594, <https://doi.org/10.1038/ncomms11594>, 2016.
- Li, H., Kupiainen-Määttä, O., Zhang, H., Zhang, X., and Ge, M.: A molecular-scale study on the role of lactic acid in new particle formation: Influence of relative humidity and temperature, *Atmos. Environ.*, 166, 479–487, <https://doi.org/10.1016/j.atmosenv.2017.07.039>, 2017.
- Li, H., Zhong, J., Vehkamäki, H., Kurteïn, T., Wang, W., Ge, M., Zhang, S., Li, Z., Zhang, X., Francisco, J. S., and Zeng, X.: Self-catalytic reaction of SO₃ and NH₃ to produce sulfuric acid and its implication to atmospheric particle formation, *J. Am. Chem. Soc.*, 140, 11020–11028, <https://doi.org/10.1021/jacs.8b04928>, 2018.
- Liu, F., Bi, X., Zhang, G., Lian, X., Fu, Y., Yang, Y., Lin, Q., Jiang, F., Wang, X., Peng, P., and Sheng, G.: Gas-to-
- nen, A., Lehtipalo, K., Leiminger, M., Makhmutov, V., Mathot, S., Onnela, A., Petäjä, T., Praplan, A. P., Riccobono, F., Rissanen, M. P., Rondo, L., Schobesberger, S., Seinfeld, J. H., Steiner, G., Tomé, A., Tröstl, J., Winkler, P. M., Williamson, C., Wimmer, D., Ye, P., Baltensperger, U., Carslaw, K. S., Kulmala, M., Worsnop, D. R., and Curtius, J.: Neutral molecular cluster formation of sulfuric acid–dimethylamine observed in real time under atmospheric conditions, *P. Natl. Acad. Sci. USA*, 111, 15019–15024, <https://doi.org/10.1073/pnas.1404853111>, 2014.
- Laaksonen, A., Kulmala, M., O’Dowd, C. D., Joutsensaari, J., Vaattovaara, P., Mikkonen, S., Lehtinen, K. E. J., Sogacheva, L., Dal Maso, M., Aalto, P., Petäjä, T., Sogachev, A., Yoon, Y. J., Lihavainen, H., Nilsson, D., Facchini, M. C., Cavalli, F., Fuzzi, S., Hoffmann, T., Arnold, F., Hanke, M., Sellegri, K., Umann, B., Junkermann, W., Coe, H., Allan, J. D., Alfarra, M. R., Worsnop, D. R., Riekkola, M.-L., Hyötyläinen, T., and Viisanen, Y.: The role of VOC oxidation products in continental new particle formation, *Atmos. Chem. Phys.*, 8, 2657–2665, <https://doi.org/10.5194/acp-8-2657-2008>, 2008.
- Lee, S. H., Gordon, H., Yu, H., Lehtipalo, K., Haley, R., Li, Y., and Zhang, R.: New Particle Formation in the Atmosphere: From Molecular Clusters to Global Climate, *J. Geophys. Res.-Atmos.*, 124, 7098–7146, <https://doi.org/10.1029/2018JD029356>, 2019.
- Lehtinen, K. E. J., Dal Maso, M., Kulmala, M., and Kerminen, V.-M.: Estimating nucleation rates from apparent particle formation rates and vice versa: Revised formulation of the Kerminen–Kulmala equation, *J. Aerosol Sci.*, 38, 988–994, <https://doi.org/10.1016/j.jaerosci.2007.06.009>, 2007.
- Lehtipalo, K., Rondo, L., Kontkanen, J., Schobesberger, S., Jokinen, T., Sarnela, N., Kürten, A., Ehrhart, S., Franchin, A., Nieminen, T., Riccobono, F., Sipilä, M., Yli-Juuti, T., Duplissy, J., Adamov, A., Ahlm, L., Almeida, J., Amorim, A., Bianchi, F., Breitenlechner, M., Dommen, J., Downard, A. J., Dunne, E. M., Flagan, R. C., Guida, R., Hakala, J., Hansel, A., Jud, W., Kangasluoma, J., Kerminen, V.-M., Keskinen, H., Kim, J., Kirkby, J., Kupc, A., Kupiainen-Määttä, O., Laaksonen, A., Lawler, M. J., Leiminger, M., Mathot, S., Olenius, T., Ortega, I. K., Onnela, A., Petäjä, T., Praplan, A., Rissanen, M. P., Ruuskanen, T., Santos, F. D., Schallhart, S., Schnitzhofer, R., Simon, M., Smith, J. N., Tröstl, J., Tsagkogeorgas, G., Tomé, A., Vaattovaara, P., Vehkamäki, H., Vrtala, A. E., Wagner, P. E., Williamson, C., Wimmer, D., Winkler, P. M., Virtanen, A., Donahue, N. M., Carslaw, K. S., Baltensperger, U., Riipinen, I., Curtius, J., Worsnop, D. R., and Kulmala, M.: The effect of acid–base clustering and ions on the growth of atmospheric nano-particles, *Nat. Commun.*, 7, 11594, <https://doi.org/10.1038/ncomms11594>, 2016.

- particle partitioning of atmospheric amines observed at a mountain site in southern China, *Atmos. Environ.*, 195, 1–11, <https://doi.org/10.1016/j.atmosenv.2018.09.038>, 2018.
- Liu, J. R., Liu, L., Rong, H., and Zhang, X. H.: The potential mechanism of atmospheric new particle formation involving amino acids with multiple functional groups, *Phys. Chem. Chem. Phys.*, 23, 10184–10195, <https://doi.org/10.1039/d0cp06472f>, 2021.
- Liu, L., Zhang, X., Li, Z., Zhang, Y., and Ge, M.: Gas-phase hydration of glyoxylic acid: Kinetics and atmospheric implications, *Chemosphere*, 186, 430–437, <https://doi.org/10.1016/j.chemosphere.2017.08.007>, 2017.
- Liu, L., Kupiainen-Maatta, O., Zhang, H. J., Li, H., Zhong, J., Kurten, T., Vehkamäki, H., Zhang, S. W., Zhang, Y. H., Ge, M., Zhang, X. H., and Li, Z. S.: Clustering mechanism of oxocarboxylic acids involving hydration reaction: Implications for the atmospheric models, *J. Chem. Phys.*, 148, 214303, <https://doi.org/10.1063/1.5030665>, 2018.
- Liu, L., Zhong, J., Vehkamäki, H., Kurtén, T., Du, L., Zhang, X., Francisco, J. S., and Zeng, X.-C.: Unexpected quenching effect on new particle formation from the atmospheric reaction of methanol with SO₃, *P. Natl. Acad. Sci. USA*, 116, 24966–24971, <https://doi.org/10.1073/pnas.1915459116>, 2019.
- Liu, L., Yu, F., Du, L., Yang, Z., Francisco, J. S., and Zhang, X.: Rapid sulfuric acid–dimethylamine nucleation enhanced by nitric acid in polluted regions, *P. Natl. Acad. Sci. USA*, 118, e2108384118, <https://doi.org/10.1073/pnas.2108384118>, 2021.
- Loukonen, V., Kurtén, T., Ortega, I. K., Vehkamäki, H., Pádua, A. A. H., Sellegri, K., and Kulmala, M.: Enhancing effect of dimethylamine in sulfuric acid nucleation in the presence of water – a computational study, *Atmos. Chem. Phys.*, 10, 4961–4974, <https://doi.org/10.5194/acp-10-4961-2010>, 2010.
- Lu, T.: Molclus Program, Version 1.9.9.9, <http://www.keinsci.com/research/molclus.html>, last access: 6 March 2022.
- Lv, G., Sui, X., Chen, J., Jayaratne, R., and Mellouki, A.: Investigation of new particle formation at the summit of Mt. Tai, China, *Atmos. Chem. Phys.*, 18, 2243–2258, <https://doi.org/10.5194/acp-18-2243-2018>, 2018.
- Ma, F., Xie, H.-B., Elm, J., Shen, J., Chen, J., and Vehkamäki, H.: Piperazine enhancing sulfuric acid-based new particle formation: implications for the atmospheric fate of piperazine, *Environ. Sci. Technol.*, 53, 8785–8795, <https://doi.org/10.1021/acs.est.9b02117>, 2019.
- Mackenzie, R. B., Dewberry, C. T., and Leopold, K. R.: Gas phase observation and microwave spectroscopic characterization of formic sulfuric anhydride, *Science*, 349, 58–61, <https://doi.org/10.1126/science.aaa9704>, 2015.
- Matsumoto, K., Kuwabara, T., and Nakano, T.: Seasonal trends and potential sources of aliphatic amines in the aerosols and gas phase at a forested site on the northern foot of Mt. Fuji, Japan, *Atmos. Environ.*, 309, 119885, <https://doi.org/10.1016/j.atmosenv.2023.119885>, 2023.
- McGrath, M. J., Olenius, T., Ortega, I. K., Loukonen, V., Paasonen, P., Kurtén, T., Kulmala, M., and Vehkamäki, H.: Atmospheric Cluster Dynamics Code: a flexible method for solution of the birth-death equations, *Atmos. Chem. Phys.*, 12, 2345–2355, <https://doi.org/10.5194/acp-12-2345-2012>, 2012.
- McNeill, V. F.: Aqueous Organic Chemistry in the Atmosphere: Sources and Chemical Processing of Organic Aerosols, *Environ. Sci. Technol.*, 49, 1237–1244, <https://doi.org/10.1021/es5043707>, 2015.
- McNeill, V. F., Woo, J. L., Kim, D. D., Schwier, A. N., Wannell, N. J., Sumner, A. J., and Barakat, J. M.: Aqueous-phase secondary organic aerosol and organosulfate formation in atmospheric aerosols: A Modeling Study, *Environ. Sci. Technol.*, 46, 8075–8081, <https://doi.org/10.1021/es3002986>, 2012.
- Metzger, A., Verheggen, B., Dommen, J., Duplissy, J., Prevot, A. S. H., Weingartner, E., Riipinen, I., Kulmala, M., Spracklen, D. V., Carslaw, K. S., and Baltensperger, U.: Evidence for the role of organics in aerosol particle formation under atmospheric conditions, *P. Natl. Acad. Sci. USA*, 107, 6646–6651, <https://doi.org/10.1073/pnas.0911330107>, 2010.
- Mikkonen, S., Romakkaniemi, S., Smith, J. N., Korhonen, H., Petäjä, T., Plass-Duelmer, C., Boy, M., McMurry, P. H., Lehtinen, K. E. J., Joutsensaari, J., Hamed, A., Mauldin III, R. L., Birmili, W., Spindler, G., Arnold, F., Kulmala, M., and Laaksonen, A.: A statistical proxy for sulphuric acid concentration, *Atmos. Chem. Phys.*, 11, 11319–11334, <https://doi.org/10.5194/acp-11-11319-2011>, 2011.
- Mitsui, Y., Imada, N., Kikkawa, H., and Katagawa, A.: Study of Hg and SO₃ behavior in flue gas of oxy-fuel combustion system, *Int. J. Greenh. Gas Con.*, 5, S143–S150, <https://doi.org/10.1016/j.ijggc.2011.05.017>, 2011.
- Miyazaki, Y., Sawano, M., and Kawamura, K.: Low-molecular-weight hydroxyacids in marine atmospheric aerosol: evidence of a marine microbial origin, *Biogeosciences*, 11, 4407–4414, <https://doi.org/10.5194/bg-11-4407-2014>, 2014.
- Mochizuki, T., Kawamura, K., Aoki, K., and Sugimoto, N.: Long-range atmospheric transport of volatile monocarboxylic acids with Asian dust over a high mountain snow site, central Japan, *Atmos. Chem. Phys.*, 16, 14621–14633, <https://doi.org/10.5194/acp-16-14621-2016>, 2016.
- Mochizuki, T., Kawamura, K., Nakamura, S., Kanaya, Y., and Wang, Z.: Enhanced levels of atmospheric low-molecular weight monocarboxylic acids in gas and particulates over Mt. Tai, North China, during field burning of agricultural wastes, *Atmos. Environ.*, 171, 237–247, <https://doi.org/10.1016/j.atmosenv.2017.10.026>, 2017.
- Mochizuki, T., Kawamura, K., Miyazaki, Y., Kunwar, B., and Boreddy, S. K. R.: Distributions and sources of low-molecular-weight monocarboxylic acids in gas and particles from a deciduous broadleaf forest in northern Japan, *Atmos. Chem. Phys.*, 19, 2421–2432, <https://doi.org/10.5194/acp-19-2421-2019>, 2019.
- Mutzel, A., Poulain, L., Berndt, T., Iinuma, Y., Rodigast, M., Böge, O., Richters, S., Spindler, G., Sipilä, M., Jokinen, T., Kulmala, M., and Herrmann, H.: Highly Oxidized Multifunctional Organic Compounds Observed in Tropospheric Particles: A Field and Laboratory Study, *Environ. Sci. Technol.*, 49, 7754–7761, <https://doi.org/10.1021/acs.est.5b00885>, 2015.
- Neese, F.: The ORCA program system, *WIREs Comput. Mol. Sci.*, 2, 73–78, <https://doi.org/10.1002/wcms.81>, 2012.
- Nguyen, Q. T., Christensen, M. K., Cozzi, F., Zare, A., Hansen, A. M. K., Kristensen, K., Tulinius, T. E., Madsen, H. H., Christensen, J. H., Brandt, J., Massling, A., Nøjgaard, J. K., and Glasius, M.: Understanding the anthropogenic influence on formation of biogenic secondary organic aerosols in Denmark via analysis of organosulfates and related oxidation products, *At-*

- mos. Chem. Phys., 14, 8961–8981, <https://doi.org/10.5194/acp-14-8961-2014>, 2014.
- Ning, A. and Zhang, X.: The synergistic effects of methanesulfonic acid (MSA) and methanesulfinic acid (MSIA) on marine new particle formation, *Atmos. Environ.*, 269, 118826, <https://doi.org/10.1016/j.atmosenv.2021.118826>, 2022.
- Ning, A., Zhang, H., Zhang, X., Li, Z., Zhang, Y., Xu, Y., and Ge, M.: A molecular-scale study on the role of methanesulfinic acid in marine new particle formation, *Atmos. Environ.*, 227, 117378, <https://doi.org/10.1016/j.atmosenv.2020.117378>, 2020.
- O'Dowd, C. D., Aalto, P., Hmeri, K., Kulmala, M., and Hoffmann, T.: Atmospheric particles from organic vapours, *Nature*, 416, 497–498, <https://doi.org/10.1038/416497a>, 2002.
- Olenius, T., Kupiainen-Määttä, O., Ortega, I., Kurtén, T., and Vehkamäki, H.: Free energy barrier in the growth of sulfuric acid–ammonia and sulfuric acid–dimethylamine clusters, *J. Chem. Phys.*, 139, 084312, <https://doi.org/10.1063/1.4819024>, 2013.
- Olenius, T., Halonen, R., Kurtén, T., Henschel, H., Kupiainen-Määttä, O., Ortega, I. K., Jen, C. N., Vehkamäki, H., and Riipinen, I.: New particle formation from sulfuric acid and amines: Comparison of monomethylamine, dimethylamine, and trimethylamine, *J. Geophys. Res.-Atoms.*, 122, 7103–7118, <https://doi.org/10.1002/2017JD026501>, 2017.
- Olson, C. N., Galloway, M. M., Yu, G., Hedman, C. J., Lockett, M. R., Yoon, T., Stone, E. A., Smith, L. M., and Keutsch, F. N.: Hydroxycarboxylic Acid-Derived Organosulfates: Synthesis, Stability, and Quantification in Ambient Aerosol, *Environ. Sci. Technol.*, 45, 6468–6474, <https://doi.org/10.1021/es201039p>, 2011.
- Ortega, I. K., Kupiainen, O., Kurtén, T., Olenius, T., Wilkman, O., McGrath, M. J., Loukonen, V., and Vehkamäki, H.: From quantum chemical formation free energies to evaporation rates, *Atmos. Chem. Phys.*, 12, 225–235, <https://doi.org/10.5194/acp-12-225-2012>, 2012.
- Passananti, M., Kong, L., Shang, J., Dupart, Y., Perrier, S., Chen, J., Donaldson, D. J., and George, C.: Organosulfate Formation through the Heterogeneous Reaction of Sulfur Dioxide with Unsaturated Fatty Acids and Long-Chain Alkenes, *Angew. Chem. Int. Edit.*, 55, 10336–10339, <https://doi.org/10.1002/anie.201605266>, 2016.
- Riipinen, I., Sihto, S.-L., Kulmala, M., Arnold, F., Dal Maso, M., Birmili, W., Saarnio, K., Teinilä, K., Kerminen, V.-M., Laaksonen, A., and Lehtinen, K. E. J.: Connections between atmospheric sulphuric acid and new particle formation during QUEST III–IV campaigns in Heidelberg and Hyytiälä, *Atmos. Chem. Phys.*, 7, 1899–1914, <https://doi.org/10.5194/acp-7-1899-2007>, 2007.
- Riplinger, C. and Neese, F.: An efficient and near linear scaling pair natural orbital based local coupled cluster method, *J. Chem. Phys.*, 138, 034106, <https://doi.org/10.1063/1.4773581>, 2013.
- Riplinger, C., Sandhoefer, B., Hansen, A., and Neese, F.: Natural triple excitations in local coupled cluster calculations with pair natural orbitals, *J. Chem. Phys.*, 139, 134101, <https://doi.org/10.1063/1.4821834>, 2013.
- Ristovski, Z. D., Suni, T., Kulmala, M., Boy, M., Meyer, N. K., Duplissy, J., Turnipseed, A., Morawska, L., and Baltensperger, U.: The role of sulphates and organic vapours in growth of newly formed particles in a eucalypt forest, *Atmos. Chem. Phys.*, 10, 2919–2926, <https://doi.org/10.5194/acp-10-2919-2010>, 2010.
- Riva, M., Tomaz, S., Cui, T., Lin, Y.-H., Perraudin, E., Gold, A., Stone, E. A., Villenave, E., and Surratt, J. D.: Evidence for an Unrecognized Secondary Anthropogenic Source of Organosulfates and Sulfonates: Gas-Phase Oxidation of Polycyclic Aromatic Hydrocarbons in the Presence of Sulfate Aerosol, *Environ. Sci. Technol.*, 49, 6654–6664, <https://doi.org/10.1021/acs.est.5b00836>, 2015.
- Riva, M., Budisulistiorini, S. H., Chen, Y., Zhang, Z., D'Ambro, E. L., Zhang, X., Gold, A., Turpin, B. J., Thornton, J. A., Canagaratna, M. R., and Surratt, J. D.: Chemical Characterization of Secondary Organic Aerosol from Oxidation of Isoprene Hydroxyhydroperoxides, *Environ. Sci. Technol.*, 50, 9889–9899, <https://doi.org/10.1021/acs.est.6b02511>, 2016.
- Rong, H., Liu, L., Liu, J., and Zhang, X.: Glyoxylic sulfuric anhydride from the gas-phase reaction between glyoxylic acid and SO₃: a potential nucleation precursor, *J. Phys. Chem. A*, 124, 3261–3268, <https://doi.org/10.1021/acs.jpca.0c01558>, 2020.
- Rose, C., Zha, Q., Dada, L., Yan, C., Lehtipalo, K., Junninen, H., Mazon, S. B., Jokinen, T., Sarnela, N., Sipilä, M., Petäjä, T., Kerminen, V.-M., Bianchi, F., and Kulmala, M.: Observations of biogenic ion-induced cluster formation in the atmosphere, *Sci. Adv.*, 4, eaar5218, <https://doi.org/10.1126/sciadv.aar5218>, 2018.
- Shakya, K. M. and Peltier, R. E.: Non-sulfate sulfur in fine aerosols across the United States: Insight for organosulfate prevalence, *Atmos. Environ.*, 100, 159–166, <https://doi.org/10.1016/j.atmosenv.2014.10.058>, 2015.
- Shampine, L. F. and Reichelt, M. W.: The MATLAB ODE Suite, *SIAM J. Sci. Comput.*, 18, 1–22, <https://doi.org/10.1137/s1064827594276424>, 1997.
- Shen, G., Suto, M., and Lee, L. C.: Reaction rate constant of SO₃+CH₃OH in the gas phase, *Int. J. Chem. Kinet.*, 22, 633–639, <https://doi.org/10.1002/kin.550220607>, 1990.
- Shen, J., Xie, H.-B., Elm, J., Ma, F., Chen, J., and Vehkamäki, H.: Methanesulfonic Acid-driven New Particle Formation Enhanced by Monoethanolamine: A Computational Study, *Environ. Sci. Technol.*, 53, 14387–14397, <https://doi.org/10.1021/acs.est.9b05306>, 2019.
- Shen, J., Elm, J., Xie, H.-B., Chen, J., Niu, J., and Vehkamäki, H.: Structural Effects of Amines in Enhancing Methanesulfonic Acid-Driven New Particle Formation, *Environ. Sci. Technol.*, 54, 13498–13508, <https://doi.org/10.1021/acs.est.0c05358>, 2020.
- Sipilä, M., Berndt, T., Petäjä, T., Brus, D., Vanhanen, J., Stratmann, F., Patokoski, J., Mauldin, R. L., Hyvärinen, A. P., Lihavainen, H., and Kulmala, M.: The Role of Sulfuric Acid in Atmospheric Nucleation, *Science*, 327, 1243–1246, <https://doi.org/10.1126/science.1180315>, 2010.
- Smith, C., Huff, A. K., Ward, R. M., and Leopold, K. R.: Carboxylic Sulfuric Anhydrides, *J. Phys. Chem. A*, 124, 601–612, <https://doi.org/10.1021/acs.jpca.9b09310>, 2019.
- Smith, C. J., Huff, A. K., Mackenzie, R. B., and Leopold, K. R.: Observation of Two Conformers of Acrylic Sulfuric Anhydride by Microwave Spectroscopy, *J. Phys. Chem. A*, 121, 9074–9080, <https://doi.org/10.1021/acs.jpca.7b09833>, 2017.
- Smith, C. J., Huff, A. K., Mackenzie, R. B., and Leopold, K. R.: Hydration of an Acid Anhydride: The Water Complex of Acetic Sulfuric Anhydride, *J. Phys. Chem. A*, 122, 4549–4554, <https://doi.org/10.1021/acs.jpca.8b02432>, 2018.

- Stewart, J. J. P.: Optimization of parameters for semiempirical methods V: Modification of NDDO approximations and application to 70 elements, *J. Mol. Model.*, 13, 1173–1213, <https://doi.org/10.1007/s00894-007-0233-4>, 2007.
- Stewart, J. J. P.: Optimization of parameters for semiempirical methods VI: more modifications to the NDDO approximations and re-optimization of parameters, *J. Mol. Model.*, 19, 1–32, <https://doi.org/10.1007/s00894-012-1667-x>, 2013.
- Stewart, J. J. P.: MOPAC2016, Colorado Springs, CO, USA, 2016.
- Stieger, B., van Pinxteren, D., Tilgner, A., Spindler, G., Poulain, L., Grüner, A., Wallasch, M., and Herrmann, H.: Strong deviations from thermodynamically expected phase partitioning of low-molecular-weight organic acids during one year of rural measurements, *ACS Earth Space Chem.*, 5, 500–515, <https://doi.org/10.1021/acsearthspacechem.0c00297>, 2021.
- Tan, S., Chen, X., and Yin, S.: Comparison results of eight oxygenated organic molecules: Unexpected contribution to new particle formation in the atmosphere, *Atmos. Environ.*, 268, 118817, <https://doi.org/10.1016/j.atmosenv.2021.118817>, 2022a.
- Tan, S., Zhang, X., Lian, Y., Chen, X., Yin, S., Du, L., and Ge, M.: OH group orientation leads to organosulfate formation at the liquid aerosol surface, *J. Am. Chem. Soc.*, 144, 16953–16964, <https://doi.org/10.1021/jacs.2c05807>, 2022b.
- Tan, X.-F., Long, B., Ren, D.-S., Zhang, W.-J., Long, Z.-W., and Mitchell, E.: Atmospheric chemistry of CH₃CHO: the hydrolysis of CH₃CHO catalyzed by H₂SO₄, *Phys. Chem. Chem. Phys.*, 20, 7701–7709, <https://doi.org/10.1039/C7CP07312G>, 2018.
- Tolocka, M. P. and Turpin, B.: Contribution of organosulfur compounds to organic aerosol mass, *Environ. Sci. Technol.*, 46, 7978–7983, <https://doi.org/10.1021/es300651v>, 2012.
- Wang, L., Khalizov, A. F., Zheng, J., Xu, W., Ma, Y., Lal, V., and Zhang, R.: Atmospheric nanoparticles formed from heterogeneous reactions of organics, *Nat. Geosci.*, 3, 238–242, <https://doi.org/10.1038/ngeo778>, 2010.
- Wang, M. Y., Kong, W. M., Marten, R., He, X. C., Chen, D. X., Pfeifer, J., Heitto, A., Kontkanen, J., Dada, L., Kurten, A., Yli-Juuti, T., Manninen, H. E., Amanatidis, S., Amorim, A., Baalbaki, R., Baccarini, A., Bell, D. M., Bertozzi, B., Brakling, S., Brilke, S., Murillo, L. C., Chiu, R., Chu, B. W., De Menezes, L. P., Duplissy, J., Finkenzeller, H., Carracedo, L. G., Granzin, M., Guida, R., Hansel, A., Hofbauer, V., Krechmer, J., Lehtipalo, K., Lamkaddam, H., Lampimäki, M., Lee, C. P., Makhmutov, V., Marie, G., Mathot, S., Mauldin, R. L., Mentler, B., Müller, T., Onnela, A., Partoll, E., Petaja, T., Philippov, M., Pospisilova, V., Ranjithkumar, A., Rissanen, M., Rorup, B., Scholz, W., Shen, J. L., Simon, M., Sipila, M., Steiner, G., Stolzenburg, D., Tham, Y. J., Tome, A., Wagner, A. C., Wang, D. Y. S., Wang, Y. H., Weber, S. K., Winkler, P. M., Wlasits, P. J., Wu, Y. H., Xiao, M., Ye, Q., Zauner-Wieczorek, M., Zhou, X. Q., Volkamer, R., Riipinen, I., Dommen, J., Curtius, J., Baltensperger, U., Kulmala, M., Worsnop, D. R., Kirkby, J., Seinfeld, J. H., El-Haddad, I., Flagan, R. C., and Donahue, N. M.: Rapid growth of new atmospheric particles by nitric acid and ammonia condensation, *Nature*, 581, 184–189, <https://doi.org/10.1038/s41586-020-2270-4>, 2020.
- Wang, Y., Hu, M., Guo, S., Wang, Y., Zheng, J., Yang, Y., Zhu, W., Tang, R., Li, X., Liu, Y., Le Breton, M., Du, Z., Shang, D., Wu, Y., Wu, Z., Song, Y., Lou, S., Hallquist, M., and Yu, J.: The secondary formation of organosulfates under interactions between biogenic emissions and anthropogenic pollutants in summer in Beijing, *Atmos. Chem. Phys.*, 18, 10693–10713, <https://doi.org/10.5194/acp-18-10693-2018>, 2018.
- Wang, Y. H., Liu, Z. R., Zhang, J. K., Hu, B., Ji, D. S., Yu, Y. C., and Wang, Y. S.: Aerosol physicochemical properties and implications for visibility during an intense haze episode during winter in Beijing, *Atmos. Chem. Phys.*, 15, 3205–3215, <https://doi.org/10.5194/acp-15-3205-2015>, 2015.
- Xie, H.-B., Elm, J., Halonen, R., Myllys, N., Kurtén, T., Kulmala, M., and Vehkamäki, H.: Atmospheric fate of monoethanolamine: enhancing new particle formation of sulfuric acid as an important removal process, *Environ. Sci. Technol.*, 51, 8422–8431, <https://doi.org/10.1021/acs.est.7b02294>, 2017.
- Yao, L., Garmash, O., Bianchi, F., Zheng, J., Yan, C., Kontkanen, J., Junninen, H., Mazon, S. B., Ehn, M., and Paasonen, P.: Atmospheric new particle formation from sulfuric acid and amines in a Chinese megacity, *Science*, 361, 278–281, <https://doi.org/10.1126/science.aao4839>, 2018.
- Yao, L., Fan, X., Yan, C., Kurtén, T., Daellenbach, K. R., Li, C., Wang, Y., Guo, Y., Dada, L., Rissanen, M. P., Cai, J., Tham, Y. J., Zha, Q., Zhang, S., Du, W., Yu, M., Zheng, F., Zhou, Y., Kontkanen, J., Chan, T., Shen, J., Kujansuu, J. T., Kangasluoma, J., Jiang, J., Wang, L., Worsnop, D. R., Petäjä, T., Kerminen, V.-M., Liu, Y., Chu, B., He, H., Kulmala, M., and Bianchi, F.: Unprecedented Ambient Sulfur Trioxide (SO₃) Detection: Possible Formation Mechanism and Atmospheric Implications, *Environ. Sci. Tech. Lett.*, 7, 809–818, <https://doi.org/10.1021/acs.estlett.0c00615>, 2020.
- Ye, C., Yuan, B., Lin, Y., Wang, Z., Hu, W., Li, T., Chen, W., Wu, C., Wang, C., Huang, S., Qi, J., Wang, B., Wang, C., Song, W., Wang, X., Zheng, E., Krechmer, J. E., Ye, P., Zhang, Z., Wang, X., Worsnop, D. R., and Shao, M.: Chemical characterization of oxygenated organic compounds in the gas phase and particle phase using iodide CIMS with FIGAERO in urban air, *Atmos. Chem. Phys.*, 21, 8455–8478, <https://doi.org/10.5194/acp-21-8455-2021>, 2021.
- Ye, J., Abbatt, J. P. D., and Chan, A. W. H.: Novel pathway of SO₂ oxidation in the atmosphere: reactions with monoterpene ozonolysis intermediates and secondary organic aerosol, *Atmos. Chem. Phys.*, 18, 5549–5565, <https://doi.org/10.5194/acp-18-5549-2018>, 2018.
- Zhang, H., Worton, D. R., Lewandowski, M., Ortega, J., Rubitschun, C. L., Park, J.-H., Kristensen, K., Campuzano-Jost, P., Day, D. A., Jimenez, J. L., Jaoui, M., Offenberg, J. H., Kleindienst, T. E., Gilman, J., Kuster, W. C., de Gouw, J., Park, C., Schade, G. W., Frossard, A. A., Russell, L., Kaser, L., Jud, W., Hansel, A., Cappellin, L., Karl, T., Glasius, M., Guenther, A., Goldstein, A. H., Seinfeld, J. H., Gold, A., Kamens, R. M., and Surratt, J. D.: Organosulfates as Tracers for Secondary Organic Aerosol (SOA) Formation from 2-Methyl-3-Buten-2-ol (MBO) in the Atmosphere, *Environ. Sci. Technol.*, 46, 9437–9446, <https://doi.org/10.1021/es301648z>, 2012.
- Zhang, H., Zhang, Z., Cui, T., Lin, Y.-H., Bhathala, N. A., Ortega, J., Worton, D. R., Goldstein, A. H., Guenther, A., Jimenez, J. L., Gold, A., and Surratt, J. D.: Secondary Organic Aerosol Formation via 2-Methyl-3-buten-2-ol Photooxidation: Evidence of Acid-Catalyzed Reactive Uptake of Epoxides, *Environ. Sci. Tech. Lett.*, 1, 242–247, <https://doi.org/10.1021/ez500055f>, 2014.
- Zhang, H., Kupiainen-Määttä, O., Zhang, X., Molinero, V., Zhang, Y., and Li, Z.: The enhancement mechanism of gly-

- colic acid on the formation of atmospheric sulfuric acid–ammonia molecular clusters, *J. Chem. Phys.*, 146, 184308, <https://doi.org/10.1063/1.4982929>, 2017.
- Zhang, H., Li, H., Liu, L., Zhang, Y., Zhang, X., and Li, Z.: The potential role of malonic acid in the atmospheric sulfuric acid - Ammonia clusters formation, *Chemosphere*, 203, 26–33, <https://doi.org/10.1016/j.chemosphere.2018.03.154>, 2018.
- Zhang, H., Wang, W., Li, H., Gao, R., and Xu, Y.: A theoretical study on the formation mechanism of carboxylic sulfuric anhydride and its potential role in new particle formation, *RSC Adv.*, 12, 5501–5508, <https://doi.org/10.1039/D2RA00226D>, 2022.
- Zhang, H. J., Wang, W., Pi, S. Q., Liu, L., Li, H., Chen, Y., Zhang, Y. H., Zhang, X. H., and Li, Z. S.: Gas phase transformation from organic acid to organic sulfuric anhydride: Possibility and atmospheric fate in the initial new particle formation, *Chemosphere*, 212, 504–512, <https://doi.org/10.1016/j.chemosphere.2018.08.074>, 2018.
- Zhang, J. and Dolg, M.: ABCluster: the artificial bee colony algorithm for cluster global optimization, *Phys. Chem. Chem. Phys.*, 17, 24173–24181, <https://doi.org/10.1039/C5CP04060D>, 2015.
- Zhang, R.: Getting to the Critical Nucleus of Aerosol Formation, *Science*, 328, 1366–1367, <https://doi.org/10.1126/science.1189732>, 2010.
- Zhang, R., Suh, I., Zhao, J., Zhang, D., Fortner, E. C., Tie, X., Molina, L. T., and Molina, M. J.: Atmospheric New Particle Formation Enhanced by Organic Acids, *Science*, 304, 1487–1490, <https://doi.org/10.1126/science.1095139>, 2004.
- Zhang, R., Khalizov, A., Wang, L., Hu, M., and Xu, W.: Nucleation and Growth of Nanoparticles in the Atmosphere, *Chem. Rev.*, 112, 1957–2011, <https://doi.org/10.1021/cr2001756>, 2012.
- Zhang, R., Shen, J., Xie, H.-B., Chen, J., and Elm, J.: The role of organic acids in new particle formation from methanesulfonic acid and methylamine, *Atmos. Chem. Phys.*, 22, 2639–2650, <https://doi.org/10.5194/acp-22-2639-2022>, 2022.
- Zhang, X., Tan, S., Chen, X., and Yin, S.: Computational chemistry of cluster: Understanding the mechanism of atmospheric new particle formation at the molecular level, *Chemosphere*, 308, 136109, <https://doi.org/10.1016/j.chemosphere.2022.136109>, 2022.
- Zhao, J., Smith, J. N., Eisele, F. L., Chen, M., Kuang, C., and McMurry, P. H.: Observation of neutral sulfuric acid-amine containing clusters in laboratory and ambient measurements, *Atmos. Chem. Phys.*, 11, 10823–10836, <https://doi.org/10.5194/acp-11-10823-2011>, 2011.
- Zhong, J., Kumar, M., Francisco, J. S., and Zeng, X. C.: Insight into Chemistry on Cloud/Aerosol Water Surfaces, *Accounts Chem. Res.*, 51, 1229–1237, <https://doi.org/10.1021/acs.accounts.8b00051>, 2018.
- Zhu, M., Jiang, B., Li, S., Yu, Q., Yu, X., Zhang, Y., Bi, X., Yu, J., George, C., Yu, Z., and Wang, X.: Organosulfur Compounds Formed from Heterogeneous Reaction between SO₂ and Particulate-Bound Unsaturated Fatty Acids in Ambient Air, *Environ. Sci. Tech. Lett.*, 6, 318–322, <https://doi.org/10.1021/acs.estlett.9b00218>, 2019.
- Zhuang, Y. and Pavlish, J. H.: Fate of Hazardous Air Pollutants in Oxygen-Fired Coal Combustion with Different Flue Gas Recycling, *Environ. Sci. Technol.*, 46, 4657–4665, <https://doi.org/10.1021/es300143q>, 2012.